Split-luciferin Assay for Real-time Measurement of Cytosolic Molecular Accumulation in Live Mycobacteria

Rachita Dash[1], Andrew Spira[1], Sobika Bhandari[1], Sarah E. Newkirk[1], Noah Lucas[1], Mahendra D. Chordia[1], Marcos M. Pires[1,2*]

[1] Department of Chemistry

[2] Department of Microbiology, Immunology, and Cancer

University of Virginia

Charlottesville, VA, United States 22903

* corresponding author: mpires@virginia.edu

ABSTRACT

Tuberculosis causes over one million deaths annually and remains the leading cause of death from a single infectious agent. The emergence of multidrug-resistant *Mycobacterium tuberculosis* strains highlights the urgent need for new antibiotics, a pursuit hindered by the bacterium's complex cell envelope. As most anti-tuberculosis agents act on intracellular targets, assessing cytosolic drug accumulation is critical. Conventional approaches generally quantify whole-cell association without resolving subcellular localization. Moreover, no current method permits real-time monitoring of drug accumulation in live mycobacterial cells. Here, we present a split-luciferin-based assay to quantify molecular accumulation in mycobacteria. Using this approach, we quantified the cytosolic accumulation of diverse small-molecule antibiotics and polyarginine peptides conjugated via a disulfide-linked D-cysteine tag. We also show the localization of a polyarginine peptide inside of mycobacteria in infected macrophage cells, demonstrating that these peptides can cross multiple accumulation barriers. Our findings establish the first assay for real-time quantification of cytosolic molecular accumulation in live mycobacteria, addressing a longstanding methodological gap and enabling mechanistic insights into intracellular drug uptake.

INTRODUCTION

Tuberculosis is a major global public health concern, affecting millions annually and often considered the world's deadliest infectious disease.[1] Despite its long-standing prevalence, effective therapeutic options against the disease are limited, especially given the appearance of multidrug resistant strains.[2] Antibiotic development for tuberculosis is particularly challenging due to the complex, multilayered cell envelope of its causative agent *Mycobacterium tuberculosis* (*Mtb*).[3,4] The cell envelope includes an outer mycomembrane, an arabinogalactan layer, a peptidoglycan (PG) layer, and an inner cytoplasmic membrane.[5] To reach intracellular targets, antibiotics must traverse all of these barriers. Given that most anti-tubercular agents act on intracellular processes,[6,7] successful drug development requires not only target engagement but also a thorough understanding of a compound's ability to penetrate the cell envelope and access its site of action.

Advancing anti-tubercular drug development requires improved methodologies to assess the intracellular accumulation of compounds within mycobacterial cells.[8–15] Such approaches not only provide fundamental insights into the molecular features that govern intracellular accumulation, but also serve as practical tools for screening during high-throughput drug discovery campaigns. In pursuit of this goal, our laboratory has developed and implemented several methods to investigate molecular accumulation in bacteria,[16–21] including the Peptidoglycan Accessibility Click-Mediated AssessmeNt (PAC-MAN) assay, which employs click chemistry to quantify molecular penetration

across the mycomembrane in live mycobacteria.[22,23] While informative, PAC-MAN is limited to assessing periplasmic accumulation and does not resolve cytosolic penetration.

Liquid chromatography-tandem mass spectrometry (LC-MS/MS) remains the benchmark for quantifying whole-cell-associated molecules without chemical modification.[24,25] LC-MS/MS has been used to study the accumulation of sulfonyladenosines in *Mtb*[26] and a series of approved drugs in *Mycobacterium abscessus.*[27] However, LC-MS/MS lacks subcellular resolution, providing only bulk measurements across the entire cell. Moreover, it is limited to end-point analyses and cannot capture the temporal dynamics of accumulation. These constraints underscore the need for methodologies capable of directly assessing real-time cytosolic accumulation.

We previously developed a bioluminescence-based D-cysteine (D-cys) cytosolic accumulation assay (DCCAA) to measure cytosolic accumulation in Gram-negative bacteria.[19] Here, we adapt this approach to mycobacteria, enabling real-time quantification of cytosolic uptake.[28] The assay employs luciferase-expressing mycobacterial cells treated with 6-hydroxy-2-cyanobenzothiazole (OH-CBT) alongside test compounds tagged with a D-cys moiety *via* a disulfide linkage (**Fig. 1a**). Upon cytosolic entry, the reducing environment cleaves the disulfide bond, releasing D-cys, which rapidly undergoes biorthogonal condensation with OH-CBT *in cyto* to form D-luciferin. In turn, D-luciferin is then processed by luciferase, generating quantifiable bioluminescence (**Fig. S1a**).[29] In this study, we used DCCAA to monitor the real-time cytosolic accumulation of a range of small molecules and peptides in live mycobacteria.

This represents the first assay capable of resolving cytosolic drug uptake in real time, addressing a critical gap in current methodologies.

MAIN

Assay Development in Mycobacteria

We initially sought to build upon our prior assay parameters by employing *Mycobacterium smegmatis* (*Msm*), a model organism that recapitulates essential characteristics of the pathogenic *Mtb*.[30] Firefly luciferase was introduced into *Msm* by transformation with a previously optimized, constitutively active plasmid.[31] To confirm expression, luciferase-expressing *Msm* (*Msm (luc)*) cells were grown to mid-log phase, incubated with D-luciferin, and subsequently imaged in a multiwell plate using a gel imager. Cells harboring the plasmid exhibited strong luminescence relative to the wild-type control (*Msm (wt))*, confirming luciferase expression (**Fig. 1b**). Luminescence was also quantified after a one-hour incubation with D-luciferin using a plate reader, which also revealed a robust signal-to-noise ratio (**Fig. 1c**). These results confirmed that *Msm (luc)* exhibited a phenotype compatible with luciferase-based analysis of luciferin in these target cells.

To optimize the intensity of the luminescence signal, we evaluated luciferase activity across varying growth durations and stationary phase inoculum sizes of *Msm (luc)* cells (**Fig. 1d**). A 22-hour growth period following a 1% inoculum was found to yield a strong signal-to-background ratio and was selected as the standard condition for the assay. We also observed a correlation of luminescence (**Fig. 1d**) with cell density, which is expected since higher cell numbers result in increased photon emission across the analyzed surface area (**Fig. S2**). To confirm that the luminescence signal originated from within the

cells and was not due to an unrecognized source of extracellular luciferase activity, we separated the cells from the supernatant. *Msm (luc)* cells were incubated with D-luciferin for 30 minutes, followed by centrifugation to isolate the supernatant from the cellular pellet. After resuspension in PBST and an additional 30-minute incubation, luminescence measurements revealed near-background signal in the supernatant and a markedly stronger signal in the resuspended pellet. These results confirm that luciferin processing occurs exclusively within the cellular compartment, effectively ruling out contributions from extracellular luciferase activity (**Fig. 1e**).

We then transitioned to modeling our accumulation assay using the split luciferin system. In the assay, CBT is localized inside the target mycobacterial cell and D-cys is conjugated to a molecule of interest *via* a disulfide bond. Upon entry into the reducing cytosolic environment, the disulfide bond is cleaved, releasing free D-cys. The cytosol of mycobacteria is known to be a reducing environment, primarily due to the high intracellular concentration of mycothiol.[32–35] This unique amino acid D-cys, reacts with intracellular CBT to form D-luciferin, which is processed by luciferase to produce a luminescent signal, indicating successful cytosolic delivery. As a readily accessible proxy for our test compound conjugates, we used D-cystine, the disulfide-linked dimer of D-cys (**Fig. 2a**). Mycobacterial cells were co-incubated with OH-CBT and D-cystine and we monitored luminescence over time. Satisfyingly, we observed a robust luminescence level in *Msm (luc)* cells and no signal in *Msm-wt*, confirming the luciferase dependence of the signal observed. Uniquely, this enabled a method for monitoring accumulation over time,

which could be leveraged to elucidate how cellular factors might influence the kinetics of not only accumulation but also the cellular redox state.

We also observed a signal in the presence of free single amino acid D-cysteine. A key caveat in using free cysteine, or any thiol-containing molecule, in the oxidizing conditions of cell culture media is its rapid conversion to D-cystine, complicating attribution of observed effects to either the free thiol or its oxidized dimer (**Fig. 2b**). To test whether the amino group of D-cys is essential for its condensation with CBT, we treated cells with *N*-acetyl-D-cysteine (NAC), which lacks a free amino group. The acetylation of the *N*-terminus of this amino acid effectively prevents participation in the CBT condensation (**Fig. 2b**). Our results showed significantly reduced luminescence for NAC compared to D-cysteine. Interestingly, signals from NAC were still above background, suggesting possible endogenous *N*-deacetylase activity in mycobacterial cells. Overall, these findings highlight the requirement for free *N*-terminal cysteines in our workflow and confirm that luminescence arises from the biorthogonal reaction between OH-CBT and D-cysteine. Incubation of mycobacterial cells with OH-CBT alone with *Msm (luc)* cells also produced a detectable, albeit substantially lower, signal. We attribute this signal to the formation of L-luciferin *in cyto*, a phenomenon we previously observed in our analogous *E. coli* system.[19] Endogenous cytosolic L-cysteine (L-cys) can undergo a condensation reaction with OH-CBT to yield L-luciferin,[36–40] which has been reported to epimerize in the presence of firefly luciferase and subsequently serve as a substrate for the enzyme.[41] Indeed, treatment of *Msm (luc)* cells with L-luciferin produced luminescence signals well above background levels, indicating substantial epimerase activity when the substrate is

readily available (**Fig. 2c**). We propose that, within the context of our assay workflow, where the intracellular pool of endogenous L-cys is finite and limited, the formation of L-luciferin occurs rapidly following internalization of OH-CBT, but this pool is quickly depleted. Over time, the predominant source of cysteine for CBT condensation shifts to the D-cys tag present on molecules arriving in the cytosol.

It has been well established that the chemical nature of the substituent at the 6-position of the benzothiazole ring can significantly influence luminescence output.[42–47] Likewise, we have also previously noted this factor in luciferase based analysis.[19] Furthermore, we recognize that chemical modifications to CBT may influence their intracellular accumulation and retention within target mycobacterial cells. In light of this, we compared the luminescence signals from mycobacterial cells treated with either OH-CBT or its amino analogue, 2-cyano-6-aminobenzothiazole (NH_2-CBT) (**Fig. 2d**). Notably, these compounds are known to have differences in their reaction rate constants with L-cys, with OH-CBT reacting marginally faster.[48] Consistent with our observations in *E. coli*, NH_2-CBT yielded a higher luminescence signal in *Msm (luc)* cells. Given the faster chemical reactivity of OH-CBT, we propose that the increased luminescence observed in cells treated with NH_2-CBT stems from differences in the intracellular accumulation and retention of these compounds within mycobacterial cells. For subsequent assays, NH_2-CBT was used due to its higher luminescence signal. To establish the requirement for a reduction step in signal generation, we conducted a cell-free assay to better control and define the system's redox conditions. Specifically, we analyzed NH_2-CBT in a cell-free setup containing only the luciferase enzyme (**Fig. S3**). Luminescence was observed only

when both D-cystine and the reducing agent TCEP were present, underscoring the necessity of a reducing environment, such as that found in the cytosol, for the reaction to proceed.

We next sought to determine the optimal concentrations of assay components for use in our experiments. To this end, cells were titrated with varying concentrations of D-cystine while maintaining a constant concentration of NH_2-CBT (**Fig. 2e**). The data revealed a clear concentration-dependent increase in luminescence. Based on these results, we selected 50 μM as the working concentration of D-cystine for all subsequent assays. We then held D-cystine constant at 50 μM and performed a dose-response analysis of NH_2-CBT (**Fig. 2f**). This revealed that a labeling concentration of 50 μM NH_2-CBT provided optimal signal-to-noise levels. Accordingly, this concentration was selected for all subsequent assays. To account for background signal arising from the endogenous cysteine pool, the luminescence measured with NH_2-CBT alone was subtracted from that of D-cys tagged compounds hereon, enabling a more accurate assessment of compound accumulation patterns. Next, we set out to establish the integrity of the cell envelope upon treatment with assay components. To this end, we evaluated whether incubation of NH_2-CBT and D-cystine impacted the integrity of the *Msm* cell using Nile red, a dye previously employed to monitor mycomembrane disruption.[49–53] We observed that, in our assay, treatment of cells with NH_2-CBT and D-cystine did not significantly alter fluorescence levels, indicating that these components do not compromise cell envelope integrity and are unlikely to influence the accumulation profiles of tagged molecules (**Fig. S4**).

Collectively, these experiments established the optimal conditions for analyzing D-cys tagged compounds in luciferase-expressing mycobacteria.

Probing Determinants of Accumulation into Mycobacteria with a Model Compound

Having established the working parameters for DCCAA in mycobacteria, we next sought to broadly investigate how structural modifications to molecules or changes in cellular phenotypes (including cellular treatments) influence compound accumulation. Our first objective was to directly assess the impact of esterification on accumulation. A common prodrug strategy to mask polar functional groups, such as carboxylic acids and alcohols, involves ester formation, with the ultimate goal of enhancing biological activity in both bacterial[54] and eukaryotic systems.[55] Notably, mycobacteria are known to express esterases capable of hydrolyzing such modifications to generate the active form of the molecule in the cytosol.[56–59] Consequently, prodrug strategies could potentiate anti-mycobacterial drugs containing highly polar functional groups, provided this approach improves intracellular accumulation. This strategy may be particularly advantageous given the phagosomal localization of *Mtb* within macrophages, where esterification could facilitate passage across multiple membrane bilayers that otherwise impede drug access to molecular targets. Although ester-based modifications of antibiotics have been evaluated for anti-mycobacterial activity, their specific impact on accumulation profiles remains uncharacterized.

To empirically determine whether masking the negative charge of carboxylic acids enhances accumulation within the mycobacterial cytosol, we employed a D-cystine derivative in which both carboxylic acids were masked as methyl esters (D-cystine-ME) and performed DCCAA in *Msm (luc)* cells (**Fig. 3a and 3b**). While the esterified carboxyl group of D-cys can undergo condensation with CBT, the carboxyl group of D-luciferin must be hydrolyzed to its free acid form for proper processing by luciferase (**Fig. S1a** and **S1b**). Therefore, we anticipated that no luciferase-based signal would be detected from the parent D-cystine-ME unless the ester groups were cleaved. Indeed, in a cell-free system, luminescence signal levels in the presence of D-cystine-ME were substantially lower than those observed with the parent D-cystine (**Fig. 3a**). Moreover, luminescence signals were at background levels in the absence of a reducing agent, underscoring the requirement for disulfide bond reduction to liberate free thiols for condensation with CBT. Extending these findings to whole cells, mycobacterial cultures incubated with D-cystine-ME exhibited a marked increase in apparent accumulation over time compared to the carboxylic acid-based D-cystine (**Fig. 3b**). To the best of our knowledge, these results provide the first empirical evidence that masking carboxylic acids as ester groups can specifically enhance molecular accumulation in a manner independent of anti-mycobacterial activity. We are currently leveraging DCCAA to further investigate the substrate specificity of mycobacterial esterases.

Next, we sought to broadly assess how perturbations to the cellular environment influence compound uptake. Mycobacteria are intracellular pathogens that survive and replicate within macrophage phagosomes of the host.[60] The pH of these compartments generally

ranges from 4.5 to 6.2, depending on the state of macrophage activation.[61–64] The unique architecture of the mycobacterial cell wall is intrinsically linked to its resistance to acidic conditions.[65,66] Furthermore, mycobacteria have evolved mechanisms to sense acid stress and activate metabolic responses that maintain intracellular pH homeostasis,[67,68] disruption of which has been explored as an antimycobacterial strategy.[69] We hypothesized that changes in pH could also alter apparent accumulation, potentially enabling mycobacterial cells to restrict uptake of antimycobacterial agents upon their entry into the phagosome.

To test the impact of acidic pH, we employed DCCAA in *Msm (luc)* cells under conditions mimicking those of macrophage phagosomes to assess its influence on compound accumulation. Unexpectedly, treatment with D-luciferin resulted in a pronounced increase in luminescence signal when the pH was lowered to mimic phagosomal conditions (**Fig. 3c**). This finding was particularly surprising because it runs counter to the expected effect of pH on luciferase activity. Previous reports indicate that the quantum yield of firefly luciferase with D-luciferin generally decreases as pH is lowered; indeed, luminescence has been shown to be quenched around pH 5.6.[70] Nonetheless, the intracellular pH of mycobacteria is expected to remain relatively constant despite changes in extracellular acidity.[68,71] Next, we tested how pH changes affect signals in a split-luciferin context using D-cystine. In contrast to D-luciferin, we observed a complete loss of signal in the NH_2-CBT and D-cystine system when the pH was lowered to mimic phagosomal conditions. (**Fig. 3d**). Neither compound is expected to undergo degradation under the pH conditions employed, and our results with the parent D-luciferin confirm that luciferase expression

and processing remain functional at lower pH levels. This suggests that the accumulation of certain compounds may be particularly sensitive to changes in the extracellular pH of mycobacterial cells. While some mechanistic aspects remain unresolved, we provide the first description of how phagosomal-like pH conditions influence the apparent accumulation of molecules in mycobacteria.

It has been previously described that *Mtb* can upregulate the expression of the porin OmpATb under acidic conditions and within macrophage-internalized cells.[72] In contrast, *Msm* is thought to downregulate the transcription of the *Mycobacterium smegmatis* porin A (*mspA*) gene in response to acidic pH; this gene encodes a major porin responsible for the uptake of hydrophilic nutrients and small molecules.[73] We hypothesized that downregulation of *mspA* could reduce uptake of compounds such as D-cystine, and we set out to test this hypothesis. To this end, we employed a deletion strain *(Msm ΔmspA)* which we engineered to possess firefly luciferase *(Msm ΔmspA (luc))*. We first ensured that the deletion was maintained after the transformation using an ethidium bromide (EtBr) accumulation assay.[74] Incubation of EtBr with the *Msm ΔmspA (luc)* strain resulted in reduced fluorescence compared to *Msm (luc)*, a finding that is consistent with the loss of MspA which can promote the uptake of EtBr (**Fig. S5**). First, we tested the response of both strains to D-luciferin and found comparable luminescence signal levels across the two (**Fig. 3e**). We further examined the role of porins by comparing D-cystine and D-cystine-ME, reasoning that differences in molecular charge, which influence hydration, might affect their entry (**Fig. 3f**). Although the methyl ester consistently accumulated to higher levels in both strains, we observed no difference in accumulation upon porin

deletion. Taken together, these findings suggest that uptake of D-luciferin, D-cystine, and D -cystine-ME into the mycobacterial cytosol is likely independent of the MspA porin.

Although our data suggest that uptake of some compounds is independent of MspA, it remains possible that other porins contribute to entry. Mycobacteria encode multiple porins with overlapping or distinct substrate specificities, and compensatory mechanisms could allow alternative channels to mediate uptake under different environmental conditions.[75–77] Because the structural basis for porin-mediated uptake remains poorly understood in the field (especially for mycobacterial cells), targeting individual porins may not fully capture the contribution of porins to molecular entry. A more definitive strategy would involve employing a general approach that broadly inhibits all known porins, allowing for a clearer assessment of their collective impact on compound accumulation. Previous studies have suggested that polyamine treatment can modulate compound entry through porins in both Gram-negative bacteria[78–80] and mycobacteria.[81,82] This effect is thought to result from polyamines altering porin channel dynamics, shifting them toward a less permeable, closed configuration.[83]

To test the potential broad disruption of porins, cells were pretreated with spermidine as previously described.[82] Optical density measurements taken before and after spermidine treatment confirmed that pretreatment did not affect cell viability, consistent with previous observations in another mycobacterial species.[82] Interestingly, we observed a significant loss of signal upon incubation with D-luciferin when cells were pretreated with spermidine (**Fig. S6**). A similar effect was seen with D-cystine (**Fig. 3g**), consistent with a porin-

mediated entry mechanism for these molecules. Yet, within our assay framework, deletion of the MspA porin resulted in minimal differences in signal upon treatment with D-luciferin or D-cystine/NH_2-CBT. This discrepancy could have several explanations: spermidine may influence multiple porins, an effect not recapitulated in the *Msm ΔmspA (luc)* strain. To further investigate, we performed an EtBr uptake assay following spermidine pretreatment of both *Msm ΔmspA (luc)* and *Msm (luc)* cells (**Fig. S7**). Unexpectedly, we observed an increase in fluorescence upon spermidine addition in both strains, deviating from the anticipated decrease expected with porin blockade. This suggests that spermidine likely modulates cellular physiology through mechanisms beyond simple porin inhibition. Alternatively, deletion of MspA may trigger secondary physiological changes that remain poorly understood. For example, spermidine has been reported to influence intracellular redox homeostasis in *E. coli.*[84] Alteration of the cellular redox could influence both the reduction of D-cystine as well as the oxidation of D-luciferin which ultimately produces a luminescence signal.

There has been growing interest in identifying small-molecule adjuvants that can broadly permeabilize the mycobacterial cell envelope to enhance the uptake of potential antimycobacterial drugs. Such agents aim to overcome the formidable barrier posed by the complex mycobacterial cell wall, thereby improving drug access to intracellular targets. Among these, benzyl alcohol has received particular attention as a candidate that can disrupt envelope integrity and facilitate compound entry.[85,86] Cells were pretreated with benzyl alcohol as previously described[85] and the apparent uptake of various molecules was assessed using DCCAA. As before, optical density measurements

remained unchanged following benzyl alcohol exposure, indicating no impact on cell viability. Interestingly, our results showed that benzyl alcohol modestly reduced the accumulation of both D-luciferin (**Fig. S8**) and D-cystine/NH_2-CBT over time (**Fig. 3h**). This observation was unexpected, as membrane fluidization would typically be anticipated to facilitate compound entry and thereby increase signal. Notably, we previously observed a similar phenomenon upon treatment with polymyxin B nonapeptide (PMBN) in *E. coli*, which although is typically expected to improve accumulation[17,18], led to lower luminescence signals which we hypothesize may result from leakage of other components integral to our assay.[19]

Efflux pumps play a critical role in modulating drug accumulation and retention by actively exporting compounds out of the cell, thereby reducing their intracellular concentration and effectiveness.[87,88] These systems are often upregulated in response to stress and contribute significantly to intrinsic and acquired drug resistance in mycobacteria. To probe their impact on compound accumulation, small-molecule efflux pump inhibitors can be employed, providing a strategy to assess the contribution of active efflux to uptake and retention.[89–91] We set out to probe the effect of efflux-pump inhibitor verapamil, which was previously shown to modulate the activity of efflux pumps in mycobacterial cells.[92–94] Cells were pretreated with verapamil as described earlier,[85] and optical density measurements confirmed that treatment did not affect cell viability. However, we observed no differences in signal upon verapamil treatment, indicating that D-luciferin is likely not a substrate for the efflux pumps targeted by verapamil **(Fig S9)**.

Measuring Uptake of Antibiotics into *Mycobacteria*

We next evaluated a panel of small-molecule antibiotics with diverse physicochemical properties for their accumulation profiles mycobacteria. For each compound, a D-cys tag was added to make them compatible with DCCAA. In total, we built analogs of ciprofloxacin, puromycin, linezolid, and rifamycin B (**Fig. 4a**).[19] First, we evaluated the antibiotic conjugates cys-Puro**,** cys-Rifa**,** cys-Cipro**,** cys-Line in a cell-free system, where, in principle, they should generate equivalent luminescence signals at the same concentration, owing to the release of an identical number of D-cys moieties (**Fig. S10**).[19] In this cell-free setup, derivatives of puromycin, rifamycin B, and linezolid all generated luminescence signals of comparable magnitude, whereas the ciprofloxacin conjugate produced a markedly reduced signal (**Fig. S10**). We noted that residual covalently attached D-cys on the ciprofloxacin conjugate, following disulfide bond cleavage, could undergo a nonproductive condensation reaction with NH_2-CBT.[19]

With these results in hand, we next turned our attention to analyzing compound accumulation in live cells. All four antibiotic conjugates produced luminescence signals above background in the DCCAA assay, indicating measurable intracellular accumulation (**Fig. 4b**). For each antibiotic, the luminescence signal was approximately ten-fold lower than that observed with D-cystine, consistent with the expectation that these larger molecules would exhibit reduced apparent accumulation. At the 60-minute time point, the accumulation levels of cys-Cipro and cys-Line were comparable, whereas cys-Rifa exhibited slightly higher accumulation and cys-Puro showed the highest accumulation

among the tested conjugates (**Fig. S11**). We further analyzed the uptake of the highest accumulator in our panel, cys-Puro**,** and found its accumulation to be concentration-dependent (**Fig. 4c**). Additionally, treatment with the antibiotic conjugates at the tested concentrations did not perturb *Msm (luc)* cells, as assessed by the Nile Red assay (**Fig. S12**). Next, we sought to determine whether the accumulation of the conjugates was altered in the strain lacking MspA porin (**Fig. 4d and Fig. S13**). Previous studies have shown that the porins MspA and MspC regulate norfloxacin entry into *Msm* cells .[95] Interestingly, accumulation profiles for all four antibiotic conjugates revealed higher apparent accumulation in the *Msm ΔmspA (luc)* strain, suggesting that loss of MspA may enhance uptake or retention of these compounds. In contrast, the accumulation profile of D-luciferin remained unchanged, indicating that its uptake is not significantly influenced by the absence of MspA (**Fig. 4d**). It is worth noting that deletion of the MspA porin has been reported to cause little or no change in the MICs of rifampin (structurally similar to rifamycin) and ciprofloxacin,[95] thus being unlikely to be the port of entry of these molecules into cells. Furthermore, the MspA porin primarily facilitates the uptake of small, hydrophilic solutes.[76] However, the antibiotics in our panel, particularly when modified with a D-cys tag, are larger, which could have implications in their mode of entry into the cells.

Measuring Uptake of Polyarginine Peptides into *Mycobacteria*

One strategy for delivering cargo across cellular membranes and into the cytosol, extensively explored in mammalian systems, involves the use of cell-penetrating peptides

(CPPs).[96–99] A notable class of CPPs is polyarginines, which are composed of short, polycationic peptides that have been studied for their ability to transport diverse cargoes into the cytosol of mammalian cells[100–102] and certain bacterial cells.[103,104] Their guanidinium-rich side chains have been proposed to facilitate strong electrostatic interactions with negatively charged cell-surface components such as phosphates, promoting efficient translocation across cellular membranes.[105,106] The Wender group has demonstrated that conjugating vancomycin to a single arginine significantly enhances its bactericidal activity against mycobacterial cells.[107] In a similar context, the presence of arginine residues has been shown to be essential for the antimicrobial activity of lactoferricin-derived peptides against certain mycobacterial species.[108] While some studies have investigated the use of CPPs for delivery into bacterial cells, this remains a relatively underexplored area. Most notably, previous detection methods have primarily relied on whole-cell association – typically assessed via fluorescence microscopy – to infer uptake. However, these approaches lack direct empirical evidence confirming cytosolic localization of the peptides.

To address this gap, we empirically evaluated the uptake of a series of polyarginine peptides into the cytosol of mycobacteria using DCCAA in *Msm (luc)* cells. For polyarginine-based CPPs, previous studies have demonstrated that the number of arginine residues is a critical determinant of cellular accumulation and association levels.[109,110] To align with these structural patterns, we synthesized a library of polyarginine peptides (cysR5, cysR7, cysR9, and cysR11) each modified with an *N*-terminal D-cys moiety and a *C*-terminal tryptophan residue to facilitate peptide

quantification (**Fig. 5a**). To evaluate potential differences in the release of the D-cys tag, we first tested our polyarginine peptide series in a cell-free system under reducing conditions. As anticipated, no significant differences in luminescence signals were observed among the polyarginine peptides, suggesting that each peptide releases an equivalent amount of D-cys under reducing conditions, in the absence of barriers to intracellular accumulation. (**Fig. 5b**). We then evaluated our polyarginine series using DCCAA by treating *Msm (luc)* cells with each individual peptide and monitored the luminescence output (**Fig. 5c**). While all four peptides demonstrated noticeable apparent accumulation over the baseline, the accumulation pattern of the peptides differed markedly from that of D-cystine, displaying an initial burst-phase uptake followed by a plateau. Among the series, cysR7 displayed the highest level of accumulation, which was also found to be concentration-dependent (**Fig. 5d**). The addition of polyarginine peptides to *Msm (luc)* was also found to have minimal impact on cell envelope integrity, as determined using a Nile Red assay (**Fig. S14**). Although polyarginine uptake is generally thought to increase with the number of guanidinium groups, typically reaching a maximum at 8 to 9 arginine residues, the accumulation profiles observed in *Msm* deviated from this expected trend.

Previous studies,[111,112] including our own,[109] have demonstrated that the stereochemical configuration of polyarginine residues could play a critical role in determining peptide accumulation in mammalian cells. This effect may stem from chirality-dependent interactions at the lipid bilayer-solvent interface or other less well defined interactions at the cell surface.[113] Additionally, D-amino acids exhibit enhanced proteolytic stability,[114–116]

which may be advantageous for certain applications. To investigate the stereochemical influence on apparent accumulation in mycobacterial cells, we synthesized and evaluated a diastereomer of cysR7 (cysr7), inverting the stereochemistry at each arginine residue, in *Msm (luc)* (**Fig. S15a**). While overall accumulation levels did not differ significantly between the two peptides, their entry dynamics varied: cysR7 exhibited a more rapid decline in intracellular signal compared to cysr7 (**Fig. S15b**). These findings suggest that polyarginine uptake in mycobacteria may be largely independent of stereochemical configuration.

To further investigate the mechanism underlying polyarginine uptake, we assessed the impact of porin deletion on the accumulation of cysR7. In eukaryotic systems, CPPs are generally believed to enter cells via macropinocytosis and/or endocytic pathways.[117] We observed that in *Msm* Δ*mspA (luc)*, cysR7 accumulation had a slightly different pattern overall, whereas the accumulation of D-luciferin remained generally unchanged (**Fig. 5f**). The accumulation of cysR7 in *Msm* Δ*mspA (luc)* exhibits a modest delay in reaching peak levels compared to the wild-type *Msm (luc)*, suggesting that the MspA porin contributes, at least in part, to compound uptake. These findings highlight the value of real-time accumulation profiling, which can reveal dynamic features, such as delayed peak attainment, that are obscured in endpoint analyses.

Mycobacteria are known to persist within the phagosomal compartment of host macrophages, presenting a formidable barrier to antimicrobial delivery.[60] Before reaching the mycobacterial cell envelope, drugs must traverse two additional lipid bilayers (the

macrophage plasma membrane and the phagosomal membrane), making intracellular mycobacteria substantially more challenging to target than extracellular. Building upon our observations here that polyarginine peptides accumulate within *Msm*, we sought to determine whether such peptides also accumulate into intracellular *Msm* residing in macrophages.

To first confirm phagocytosis of mycobacteria by macrophages, we utilized a fluorescein-modified synthetic tetrapeptide PG analog developed in our lab (referred to as **PG-label** hereon), which incorporates into the PG *via* L,D-transpeptidase (Ldt)-mediated crosslinking.[118] Briefly, *Msm (wt)* were labeled with 25 μM **PG-label** and incubated with J774A.1 macrophages at a multiplicity of infection (MOI) of 100 to promote uptake (**Fig. 6a**). Flow cytometry revealed a marked increase in fluorescence in macrophages infected with PG-labeled *Msm* compared to both uninfected macrophages (**Fig. S16**) and those infected with unlabeled *Msm*, with the majority of events shifting to the bottom-right fluorescein-positive quadrant (**Fig. 6b**). Confocal microscopy further confirmed that fluorescence localized to structures consistent with intact bacterial cells within macrophages, indicating that phagocytosed *Msm* remained unlysed and structurally intact (**Fig. 6c**).

Having benchmarked the infection of macrophages with *Msm*, we next evaluated the intracellular accumulation of a fluorescent polyarginine peptide, coumR7, bearing an N-terminal coumarin moiety. Following phagocytosis of PG-labeled *Msm*, macrophages

were treated with 10 μM coumR7 for 30 min (**Fig. 6a**). Quadrant-based flow cytometry analysis demonstrated increased fluorescence in coumR7-treated cells relative to untreated controls, evident as an upward shift of events (**Fig. 6b**). In particular, for both uninfected macrophages (**Fig. S16**) and those infected with unlabeled *Msm* (**Fig. 6b**), events shifted from the bottom-left (fluorescein$^-$/coumarin$^-$) to the top-left quadrant (fluorescein$^-$/coumarin$^+$) (**Fig. 6b**). Most notably, macrophages infected with PG-labeled *Msm* exhibited a similar upward shift from the bottom-right (fluorescein$^+$/coumarin$^-$) to the top-right double-positive quadrant, which contained 84% of events (**Fig. 6b**). It is important to note that even in the absence of coumR7, macrophages harboring mycobacteria displayed a slight upward shift toward the coumarin-positive quadrants relative to macrophages alone. This is consistent with reports of *Msm* autofluorescence due to its naturally fluorescent coenzyme F_{420}, which emits a blue-green color near 475 nm when excited at 405 nm.[119] Confocal imaging further revealed that the coumarin signal from the CPP colocalized primarily with intracellular mycobacteria, with minimal signal detected in the macrophage cytosol, suggesting preferential association of coumR7 with internalized bacteria (**Fig. 6c**). Collectively, our data on CPPs provide the first direct evidence that polyarginine-based CPPs can access the cytosol of mycobacterial cells, even within the phagosomes of macrophages. This finding challenges the long-standing view of the mycobacterial envelope as an insurmountable barrier and establishes a foundation for intracellular delivery strategies in these organisms.

DISCUSSION

While antibiotic discovery efforts typically focus on optimizing chemical features that maximize potency against the intended target, less attention is often given to the compounds ability to reach that target, a factor that can be critical when the target resides within the cytosol. This imbalance may in part stem from the lack of robust and accessible tools to quantitatively assess intracellular accumulation into mycobacteria.

In this work, we present an approach to directly assess compound accumulation within the cytosol of mycobacteria, addressing a long-standing gap in the field. The strength of this method lies in its ability to distinguish true cytosolic accumulation from general cell-associated signal, a limitation common to LC-MS/MS-based assays, which typically report total cellular association rather than compartment-specific entry. Moreover, the real-time luminescent readout of this approach enables time-resolved analyses, offering insight into the kinetics of intracellular uptake. The value of such dynamic monitoring is highlighted by our observations with D-cys tagged polyarginine peptides, where accumulation patterns were nonlinear over time and would have been missed by endpoint-based measurements. However, certain limitations should be considered. First, the method relies on genetic modification, which may restrict its applicability to strains for which robust genetic tools are available. Second, the size of the tag adds molecular bulk, which could in some cases influence the uptake kinetics or subcellular distribution of the conjugated compound.

Nonetheless, our approach yielded several notable insights. For example, we were able to directly test whether perturbations to the mycobacteria or its environment that were previously reported to influence compound accumulation actually had the expected effect, providing a robust means to validate prior assumptions. We also assessed the entry of a chemically diverse panel of antibiotic conjugates into mycobacteria, revealing key differences in uptake. Expanding such assessments to a larger set of compounds could ultimately help define a "chemical grammar" for mycobacterial accumulation, guiding the rational design of future therapeutics. We also used our method to examine the uptake of D-cys tagged polyarginine peptides into mycobacteria and, to our knowledge, provide the first evidence that these peptides can enter mycobacterial cells residing within macrophages.

ACKNOWLEDGEMENT

This study was supported by the NIH grant 1R01AI178975-01 (M.M.P.), R35GM124893 (M.M.P.), and R01AI179080-01 (M.M.P.).

SUPPORTING INFORMATION

Additional figures, tables, and materials/methods are included in the supporting information file.

Competing interests

The authors declare no competing interests

Figure 1

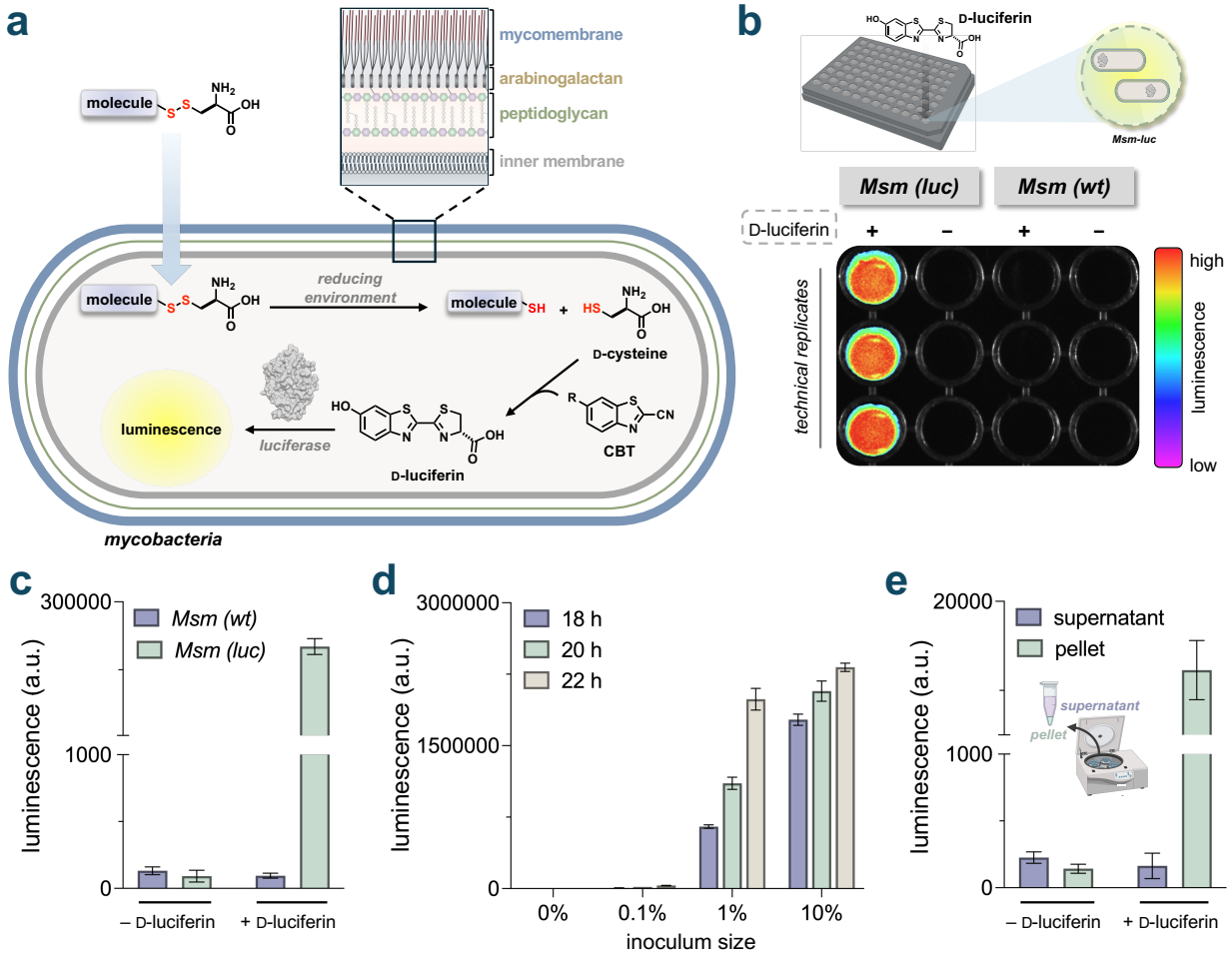

Figure 1. (a) Schematic depicting DCCAA. **(b)** Luminescent imaging of *Msm (luc)* and *Msm (wt)* cells in the presence or absence of 100 μM D-luciferin**. (c)** Quantification of the luminescence depicted in (b). **(d)** Luminescence of *Msm-luc* with varying inoculum sizes and growth durations after treatment with 25 μM D-luciferin. **(e)** Luminescence of *Msm-luc* cell pellet and supernatant after centrifugation with subsequent addition or absence of 25 μM D-luciferin. Bars in (c – e) are represented as mean ± SD (n = 3).

Figure 2

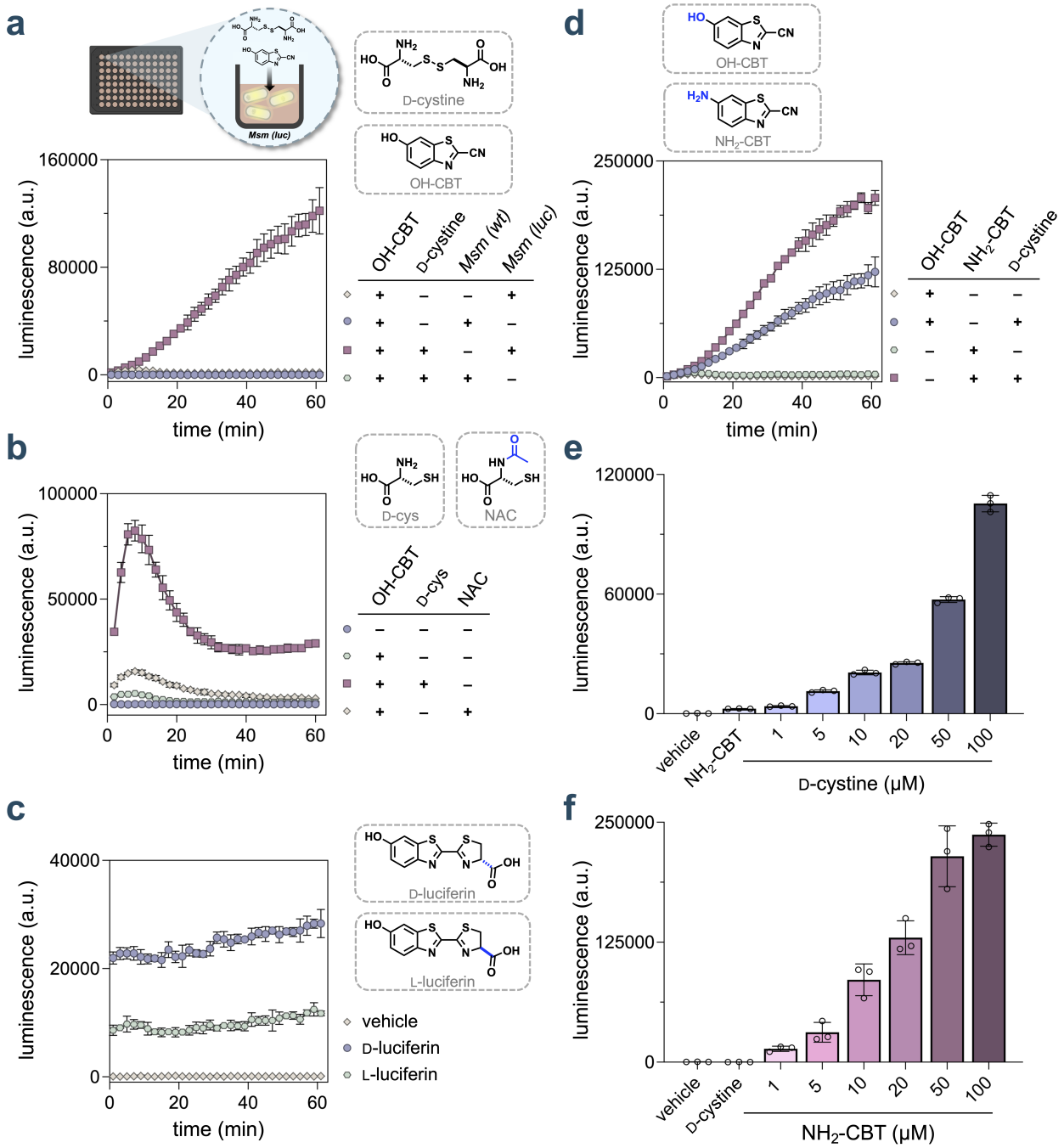

Figure 2. (a) Luminescence of *Msm (wt)* and *Msm (luc)* cells in the presence or absence of OH-CBT and D-cystine (both 50 μM). **(b – f)** Luminescence of *Msm (wt)* cells in the presence or absence of **(b)** OH-CBT, D-cys, and NAC (all 50 μM); **(c)** D- and L-luciferin (both 25 μM); **(d)** OH-CBT, NH_2-CBT, and D-cystine (all 50 μM); **(e)** D-cystine (varying

concentrations) and NH_2-CBT (50 μM); **(f)** NH_2-CBT (varying concentrations) and D-cystine (50 μM). Luminescence was measured over 60 min in (a – d) and at 60 min in (e – f) after addition of the indicated compounds. Data are represented as mean ± SD (*n* = 3).

Figure 3

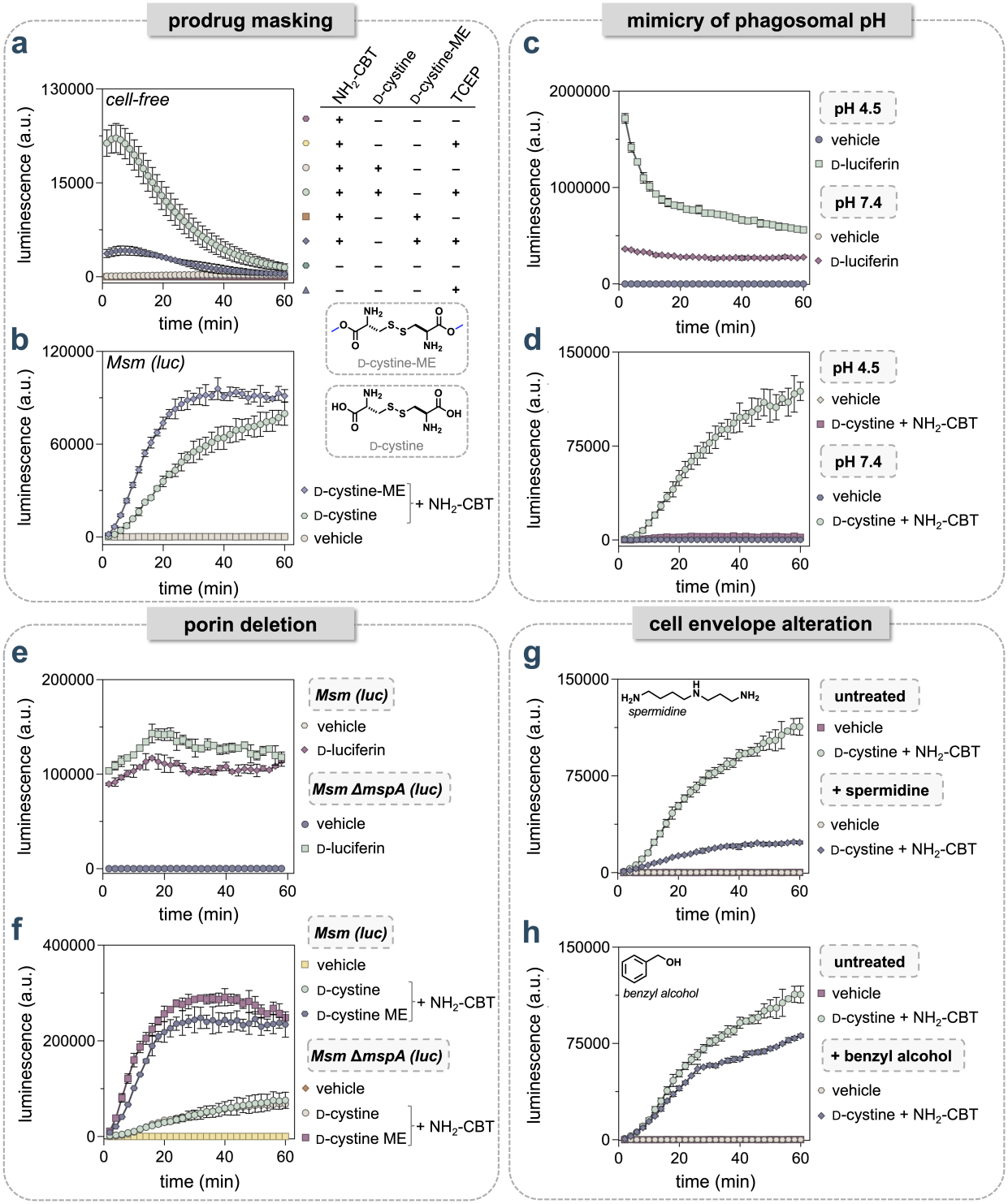

Figure 3. (a) Luminescence of *Msm (luc)* cells after addition of NH_2-CBT and either D-cystine or D-cystine-ME. **(b)** Cell-free luminescence of luciferase in the presence or

absence of NH_2-CBT, D-cystine, D-cysteine-ME, and TCEP (1 mM). **(c – d)** Luminescence of *Msm (luc)* cells in acidic (pH 4.5) and neutral (pH 7.4) buffers after addition of **(c)** D-luciferin (25 μM) or **(d)** D-cystine and NH_2-CBT. **(e – f)** Luminescence of *Msm (luc)* and *Msm ΔmspA (luc)* cells after the addition of **(e)** D-luciferin (25 μM) or **(f)** NH_2-CBT and either D-cystine or D-cystine-ME. **(g – h)** Luminescence of *Msm (luc)* cells after the addition of D-cystine and NH_2-CBT with and without **(g)** spermidine pretreatment (10 mM, 10 min) or **(h)** benzyl alcohol pretreatment (25 mM, 60 min). Luminescence was measured over 60 min after addition of the indicated compounds (all were at 50 μM unless mentioned otherwise). Data are represented as mean ± SD (n = 3).

Figure 4

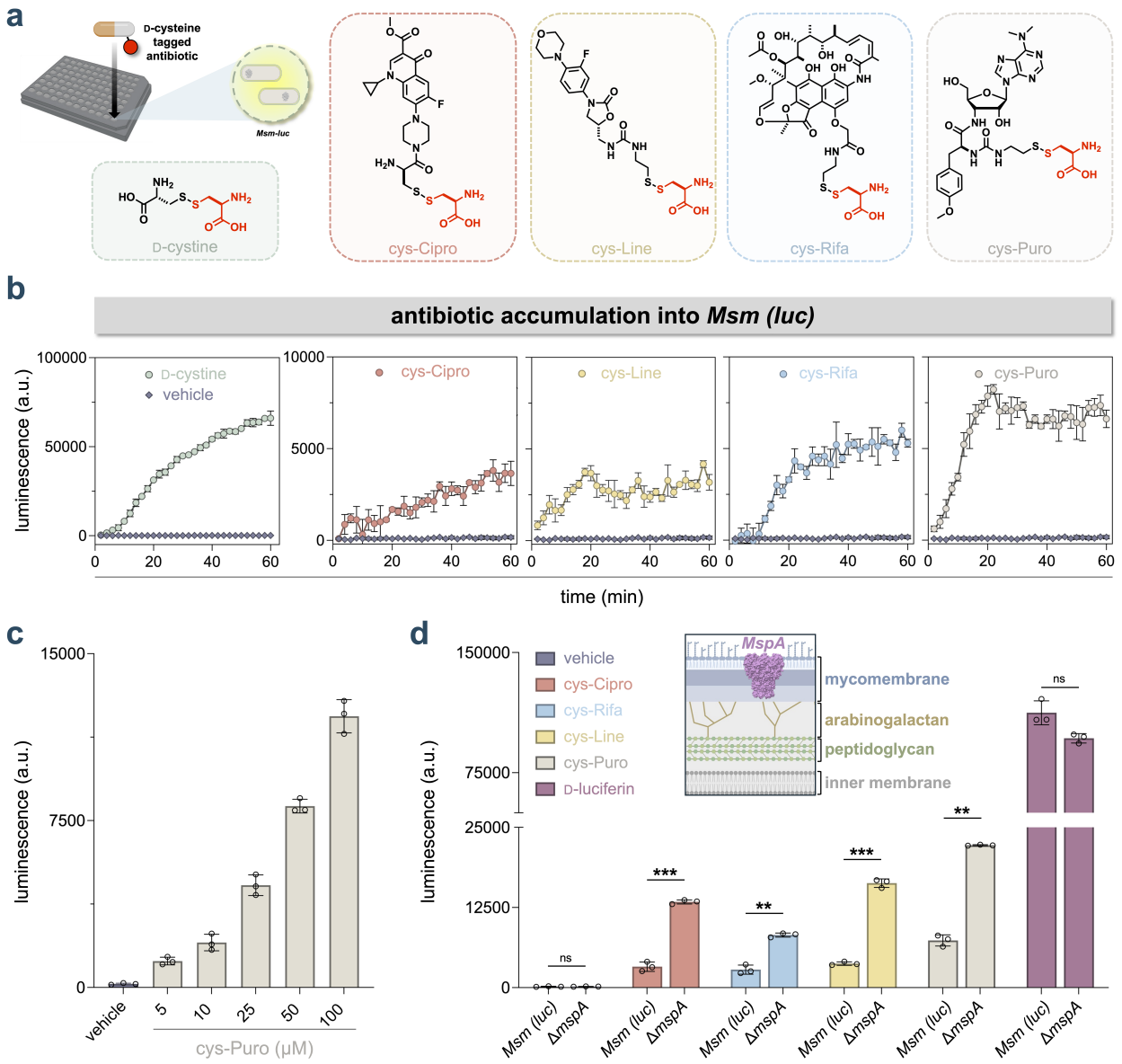

Figure 4. (a) Structures of D-cys tagged antibiotics. **(b)** Luminescence of *Msm (luc)* cells after the addition of either D-cystine or the indicated D-cys tagged antibiotic measured over 60 minutes. **(c)** Luminescence *Msm (luc)* cells 60 minutes after the addition of cys-Puro (varying concentrations). **(d)** Luminescence of *Msm (luc)* and *Msm ΔmspA (luc)* (*ΔmspA* used as shorthand) cells 60 minutes after the addition of either D-luciferin (25 μM) or the indicated D-cys tagged antibiotic (50 μM). All assays except those with D-

luciferin were done in the presence of NH_2-CBT (50 μM). All compounds were at 50 μM unless mentioned otherwise. Data are represented as mean ± SD (n = 3). P-values were determined by a two-tailed t-test (ns = not significant, *p < 0.1, **p < 0.01, ***p < 0.001).

Figure 5

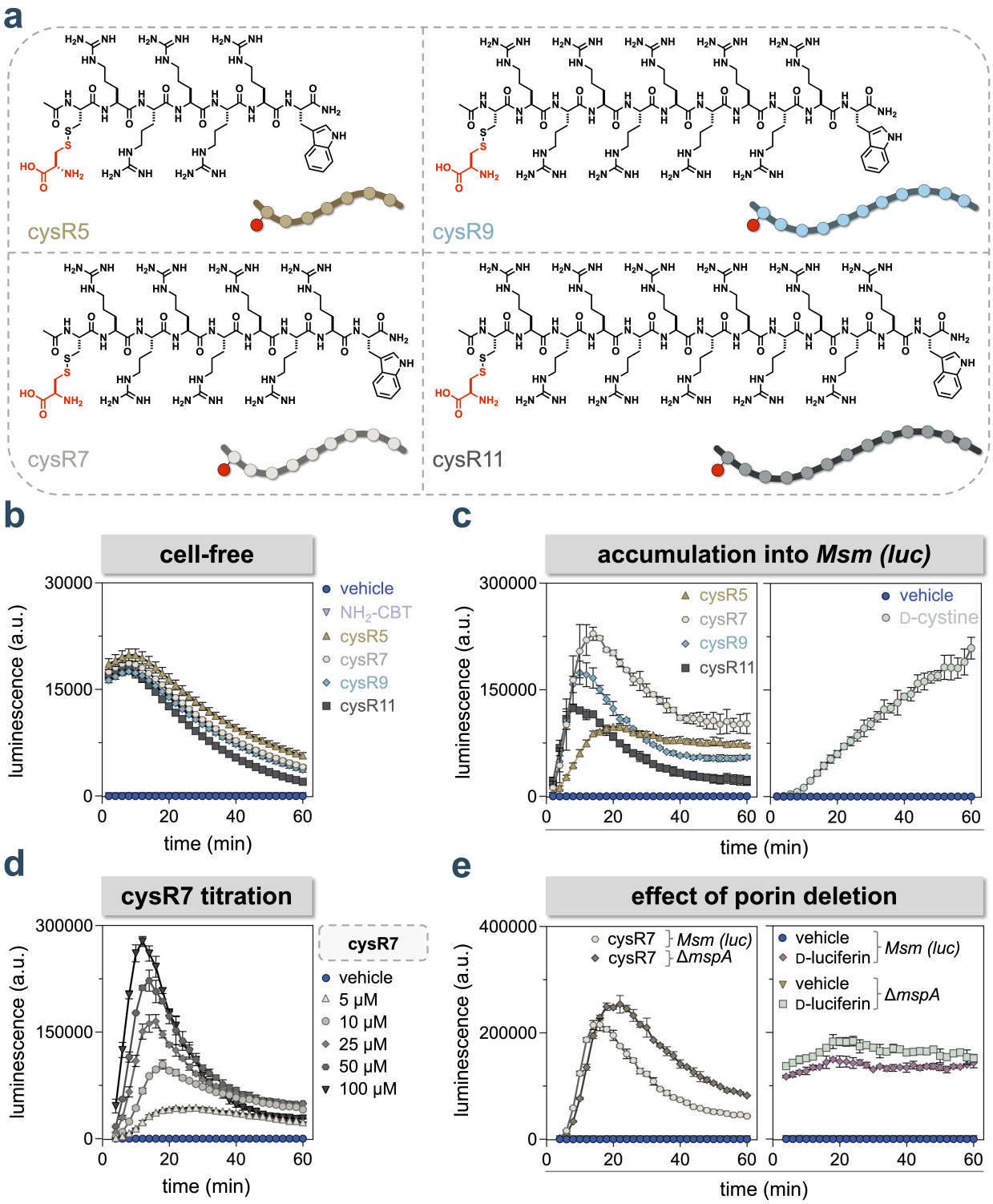

Figure 5. (a) Structures of D-cys tagged polyarginine peptides. **(b)** Cell-free luminescence of luciferase after the addition of the indicated D-cys tagged polyarginine peptide. **(c)**

Luminescence of *Msm (luc)* cells after the addition of either D-cystine or the indicated D-cys tagged polyarginine peptide. **(d)** Luminescence of *Msm (luc)* cells after the addition of NH_2-CBT and cysR7 (varying concentrations). **(e)** Luminescence of *Msm (luc)* and *Msm ΔmspA (luc)* cells after the addition of either cysR7 or D-luciferin (25 μM). All assays except those with D-luciferin were done in the presence of NH_2-CBT (50 μM). Luminescence was measured over 60 min after addition of the indicated compounds (all were at 50 μM unless mentioned otherwise). Data are represented as mean ± SD (n = 3).

Figure 6

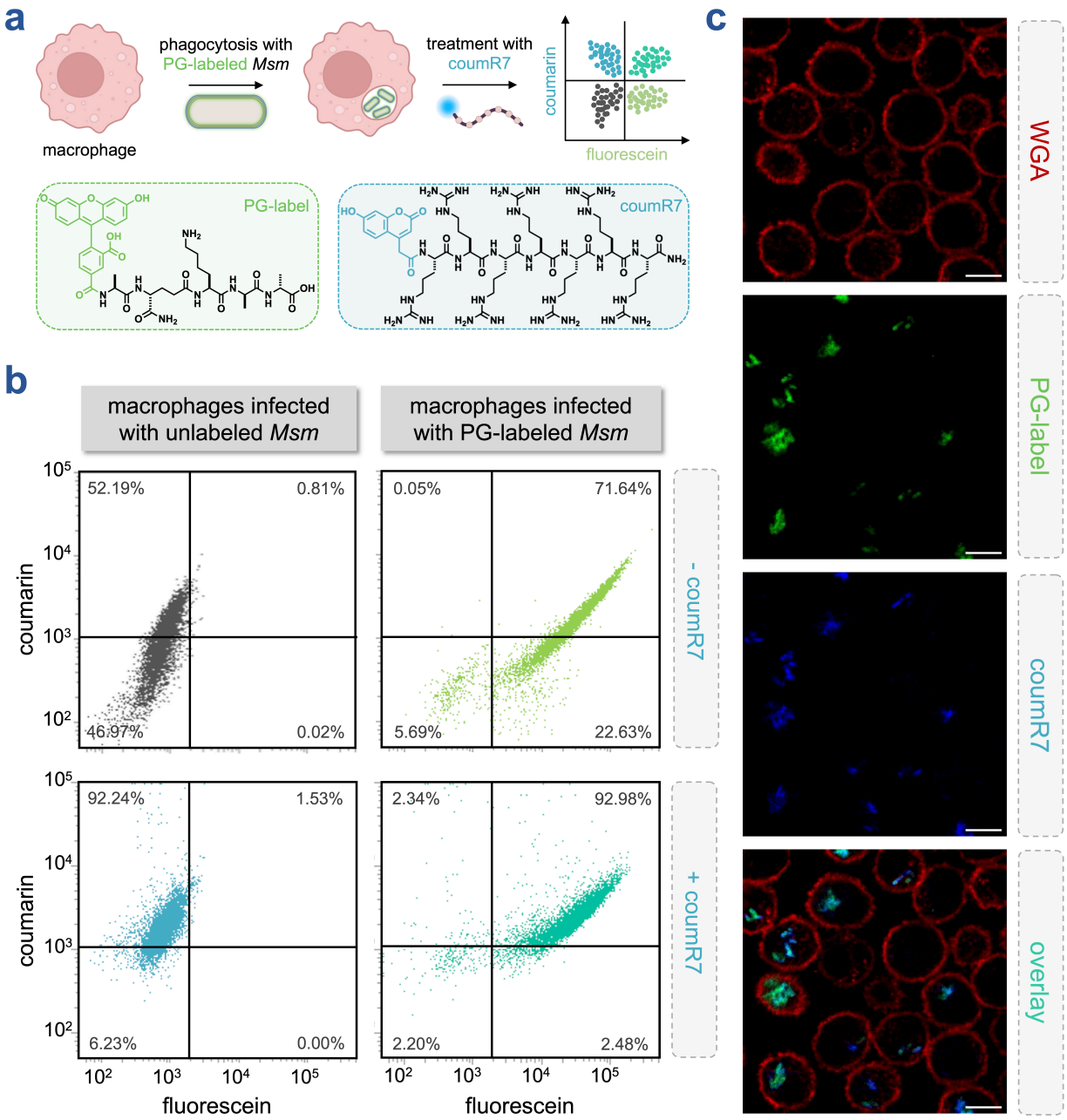

Figure 6. (a) Schematic depicting workflow for the infection assays of *Msm* in macrophages treated with coumR7. **(b)** Flow cytometry scatter plots of macrophages infected with either unlabeled or PG-labeled (25 μM) *Msm (wt)*, in the absence or presence of coumR7 (10 μM). **(c)** Confocal analysis of PG-labeled (25 μM) *Msm (wt)* in

macrophages treated with coumR7 (10 μM). Macrophage membranes were labeled with 5 μg/mL wheat germ agglutin (WGA) tetramethylrhodamine. Scale bar = 10 μm.

REFERENCES

(1) World Health Organization. *Global Tuberculosis Report 2024*. https://www.who.int/teams/global-programme-on-tuberculosis-and-lung-health/tb-reports/global-tuberculosis-report-2024/tb-disease-burden.

(2) Farhat, M.; Cox, H.; Ghanem, M.; Denkinger, C. M.; Rodrigues, C.; Abd El Aziz, M. S.; Enkh-Amgalan, H.; Vambe, D.; Ugarte-Gil, C.; Furin, J.; Pai, M. Drug-Resistant Tuberculosis: A Persistent Global Health Concern. *Nat. Rev. Microbiol.* **2024**, *22* (10), 617–635. https://doi.org/10.1038/s41579-024-01025-1.

(3) Dulberger, C. L.; Rubin, E. J.; Boutte, C. C. The Mycobacterial Cell Envelope — a Moving Target. *Nat. Rev. Microbiol.* **2020**, *18* (1), 47–59. https://doi.org/10.1038/s41579-019-0273-7.

(4) Bansal-Mutalik, R.; Nikaido, H. Mycobacterial Outer Membrane Is a Lipid Bilayer and the Inner Membrane Is Unusually Rich in Diacyl Phosphatidylinositol Dimannosides. *Proc. Natl. Acad. Sci.* **2014**, *111* (13), 4958–4963. https://doi.org/10.1073/pnas.1403078111.

(5) Chiaradia, L.; Lefebvre, C.; Parra, J.; Marcoux, J.; Burlet-Schiltz, O.; Etienne, G.; Tropis, M.; Daffé, M. Dissecting the Mycobacterial Cell Envelope and Defining the Composition of the Native Mycomembrane. *Sci. Rep.* **2017**, *7* (1), 12807. https://doi.org/10.1038/s41598-017-12718-4.

(6) Mateus, A.; Matsson, P.; Artursson, P. Rapid Measurement of Intracellular Unbound Drug Concentrations. *Mol. Pharm.* **2013**, *10* (6), 2467–2478. https://doi.org/10.1021/mp4000822.

(7) Overington, J. P.; Al-Lazikani, B.; Hopkins, A. L. How Many Drug Targets Are There? *Nat. Rev. Drug Discov.* **2006**, *5* (12), 993–996. https://doi.org/10.1038/nrd2199.

(8) Kojima, S.; Nikaido, H. Permeation Rates of Penicillins Indicate That Escherichia Coli Porins Function Principally as Nonspecific Channels. *Proc. Natl. Acad. Sci.* **2013**, *110* (28), E2629–E2634. https://doi.org/10.1073/pnas.1310333110.

(9) June, C. M.; Vaughan, R. M.; Ulberg, L. S.; Bonomo, R. A.; Witucki, L. A.; Leonard, D. A. A Fluorescent Carbapenem for Structure Function Studies of Penicillin-Binding Proteins, β-Lactamases, and β-Lactam Sensors. *Anal. Biochem.* **2014**, *463*, 70–74. https://doi.org/10.1016/j.ab.2014.07.012.

(10) Davis, T. D.; Gerry, C. J.; Tan, D. S. General Platform for Systematic Quantitative Evaluation of Small-Molecule Permeability in Bacteria. *ACS Chem. Biol.* **2014**, *9* (11), 2535–2544. https://doi.org/10.1021/cb5003015.

(11) Ghai, I.; Winterhalter, M.; Wagner, R. Probing Transport of Charged β-Lactamase Inhibitors through OmpC, a Membrane Channel from *E. Coli*. *Biochem. Biophys. Res. Commun.* **2017**, *484* (1), 51–55. https://doi.org/10.1016/j.bbrc.2017.01.076.

(12) Kaščáková, S.; Maigre, L.; Chevalier, J.; Réfrégiers, M.; Pagès, J.-M. Antibiotic Transport in Resistant Bacteria: Synchrotron UV Fluorescence Microscopy to Determine Antibiotic Accumulation with Single Cell Resolution. *PLOS ONE* **2012**, *7* (6), e38624. https://doi.org/10.1371/journal.pone.0038624.

(13) Zhou, Y.; Joubran, C.; Miller-Vedam, L.; Isabella, V.; Nayar, A.; Tentarelli, S.; Miller, A. Thinking Outside the “Bug”: A Unique Assay To Measure Intracellular Drug Penetration in Gram-Negative Bacteria. *Anal. Chem.* **2015**, *87* (7), 3579–3584. https://doi.org/10.1021/ac504880r.

(14) Cama, J.; Bajaj, H.; Pagliara, S.; Maier, T.; Braun, Y.; Winterhalter, M.; Keyser, U. F. Quantification of Fluoroquinolone Uptake through the Outer Membrane Channel OmpF of Escherichia Coli. *J. Am. Chem. Soc.* **2015**, *137* (43), 13836–13843. https://doi.org/10.1021/jacs.5b08960.

(15) Cinquin, B.; Maigre, L.; Pinet, E.; Chevalier, J.; Stavenger, R. A.; Mills, S.; Réfrégiers, M.; Pagès, J.-M. Microspectrometric Insights on the Uptake of Antibiotics at the Single Bacterial Cell Level. *Sci. Rep.* **2015**, *5* (1), 17968. https://doi.org/10.1038/srep17968.

(16) Kelly, J. J.; Dalesandro, B. E.; Liu, Z.; Chordia, M. D.; Ongwae, G. M.; Pires, M. M. Measurement of Accumulation of Antibiotics to Staphylococcus Aureus in Phagosomes of Live Macrophages. *Angew. Chem. Int. Ed.* **2024**, *63* (3), e202313870. https://doi.org/10.1002/anie.202313870.

(17) Ongwae, G. M.; Lepori, I.; Chordia, M. D.; Dalesandro, B. E.; Apostolos, A. J.; Siegrist, M. S.; Pires, M. M. Measurement of Small Molecule Accumulation into Diderm Bacteria. *ACS Infect. Dis.* **2023**, *9* (1), 97–110. https://doi.org/10.1021/acsinfecdis.2c00435.

(18) Ongwae, G. M.; Liu, Z.; Feng, S.; Chordia, M. D.; Gh, M. S.; Dash, R.; Dalesandro, B. E.; Guo, T.; Sharpless, K. B.; Dong, J.; Siegrist, M. S.; Im, W.; Pires, M. M. Click-Based Determination of Accumulation of Molecules in Escherichia Coli. bioRxiv February 24, 2025, p 2023.06.20.545103. https://doi.org/10.1101/2023.06.20.545103.

(19) Dash, R.; Holsinger, K. A.; Chordia, M. D.; Gh., M. S.; Pires, M. M. Bioluminescence-Based Determination of Cytosolic Accumulation of Antibiotics in

Escherichia Coli. *ACS Infect. Dis.* **2024**, *10* (5), 1602–1611. https://doi.org/10.1021/acsinfecdis.3c00684.

(20) Lepori, I.; Jackson, K.; Liu, Z.; Chordia, M. D.; Wong, M.; Rivera, S. L.; Roncetti, M.; Poliseno, L.; Freundlich, J. S.; Pires, M. M.; Siegrist, M. S. The Mycomembrane Differentially and Heterogeneously Restricts Antibiotic Permeation. *ACS Infect. Dis.* **2025**, *11* (7), 1893–1906. https://doi.org/10.1021/acsinfecdis.4c01062.

(21) Lepori, I.; Liu, Z.; Evbarunegbe, N.; Feng, S.; Brown, T. P.; Mane, K.; Shivangi; Wong, M.; George, A.; Guo, T.; Dong, J.; Freundlich, J. S.; Im, W.; Green, A. G.; Pires, M. M.; Siegrist, M. S. Identification of Chemical Features That Influence Mycomembrane Permeation and Antitubercular Activity. bioRxiv February 27, 2025, p 2025.02.27.640664. https://doi.org/10.1101/2025.02.27.640664.

(22) Dash, R.; Liu, Z.; Lepori, I.; Chordia, M. D.; Ocius, K.; Holsinger, K.; Zhang, H.; Kenyon, R.; Im, W.; Siegrist, M. S.; Pires, M. M. Systematic Determination of the Impact of Structural Edits on Peptide Accumulation into Mycobacteria. *ACS Chem. Biol.* **2025**, *20* (8), 1962–1979. https://doi.org/10.1021/acschembio.5c00330.

(23) Liu, Z.; Lepori, I.; Chordia, M. D.; Dalesandro, B. E.; Guo, T.; Dong, J.; Siegrist, M. S.; Pires, M. M. A Metabolic-Tag-Based Method for Assessing the Permeation of Small Molecules Across the Mycomembrane in Live Mycobacteria. *Angew. Chem. Int. Ed.* **2023**, *62* (20), e202217777. https://doi.org/10.1002/anie.202217777.

(24) Geddes, E. J.; Li, Z.; Hergenrother, P. J. An LC-MS/MS Assay and Complementary Web-Based Tool to Quantify and Predict Compound Accumulation in E. Coli. *Nat. Protoc.* **2021**, *16* (10), 4833–4854. https://doi.org/10.1038/s41596-021-00598-y.

(25) Iyer, R.; Ye, Z.; Ferrari, A.; Duncan, L.; Tanudra, M. A.; Tsao, H.; Wang, T.; Gao, H.; Brummel, C. L.; Erwin, A. L. Evaluating LC–MS/MS To Measure Accumulation of Compounds within Bacteria. *ACS Infect. Dis.* **2018**, *4* (9), 1336–1345. https://doi.org/10.1021/acsinfecdis.8b00083.

(26) Davis, T. D.; Gerry, C. J.; Tan, D. S. General Platform for Systematic Quantitative Evaluation of Small-Molecule Permeability in Bacteria. *ACS Chem. Biol.* **2014**, *9* (11), 2535–2544. https://doi.org/10.1021/cb5003015.

(27) Sullivan, M. R.; Rubin, E. J. Deep Learning-Based Prediction of Chemical Accumulation in a Pathogenic Mycobacterium. bioRxiv December 16, 2024, p 2024.12.15.628588. https://doi.org/10.1101/2024.12.15.628588.

(28) Karatas, H.; Maric, T.; D'Alessandro, P. L.; Yevtodiyenko, A.; Vorherr, T.; Hollingworth, G. J.; Goun, E. A. Real-Time Imaging and Quantification of Peptide Uptake in Vitro and in Vivo. *ACS Chem. Biol.* **2019**, *14* (10), 2197–2205. https://doi.org/10.1021/acschembio.9b00439.

(29) Godinat, A.; Bazhin, A. A.; Goun, E. A. Bioorthogonal Chemistry in Bioluminescence Imaging. *Drug Discov. Today* **2018**, *23* (9), 1584–1590. https://doi.org/10.1016/j.drudis.2018.05.022.

(30) Sparks, I. L.; Derbyshire, K. M.; Jacobs, W. R.; Morita, Y. S. Mycobacterium Smegmatis: The Vanguard of Mycobacterial Research. *J. Bacteriol.* **2023**, *205* (1), e00337-22. https://doi.org/10.1128/jb.00337-22.

(31) Andreu, N.; Zelmer, A.; Fletcher, T.; Elkington, P. T.; Ward, T. H.; Ripoll, J.; Parish, T.; Bancroft, G. J.; Schaible, U.; Robertson, B. D.; Wiles, S. Optimisation of

Bioluminescent Reporters for Use with Mycobacteria. *PLOS ONE* **2010**, *5* (5), e10777. https://doi.org/10.1371/journal.pone.0010777.

(32) den Hengst, C. D.; Buttner, M. J. Redox Control in Actinobacteria. *Biochim. Biophys. Acta BBA - Gen. Subj.* **2008**, *1780* (11), 1201–1216. https://doi.org/10.1016/j.bbagen.2008.01.008.

(33) Newton, G. L.; Buchmeier, N.; Fahey, R. C. Biosynthesis and Functions of Mycothiol, the Unique Protective Thiol of Actinobacteria. *Microbiol. Mol. Biol. Rev. MMBR* **2008**, *72* (3), 471–494. https://doi.org/10.1128/MMBR.00008-08.

(34) Newton, G. L.; Fahey, R. C. Mycothiol Biochemistry. *Arch. Microbiol.* **2002**, *178* (6), 388–394. https://doi.org/10.1007/s00203-002-0469-4.

(35) Reyes, A. M.; Pedre, B.; De Armas, M. I.; Tossounian, M.-A.; Radi, R.; Messens, J.; Trujillo, M. Chemistry and Redox Biology of Mycothiol. *Antioxid. Redox Signal.* **2018**, *28* (6), 487–504. https://doi.org/10.1089/ars.2017.7074.

(36) Van de Bittner, G. C.; Bertozzi, C. R.; Chang, C. J. Strategy for Dual-Analyte Luciferin Imaging: In Vivo Bioluminescence Detection of Hydrogen Peroxide and Caspase Activity in a Murine Model of Acute Inflammation. *J. Am. Chem. Soc.* **2013**, *135* (5), 1783–1795. https://doi.org/10.1021/ja309078t.

(37) Ren, Y.; Qiang, Y.; Zhu, B.; Tang, W.; Duan, X.; Li, Z. General Strategy for Bioluminescence Sensing of Peptidase Activity In Vivo Based on Tumor-Targeting Probiotic. *Anal. Chem.* **2021**, *93* (9), 4334–4341. https://doi.org/10.1021/acs.analchem.1c00093.

(38) Karatas, H.; Maric, T.; D'Alessandro, P. L.; Yevtodiyenko, A.; Vorherr, T.; Hollingworth, G. J.; Goun, E. A. Real-Time Imaging and Quantification of Peptide

Uptake in Vitro and in Vivo. *ACS Chem. Biol.* **2019**, *14* (10), 2197–2205. https://doi.org/10.1021/acschembio.9b00439.

(39) Niwa, K.; Nakamura, M.; Ohmiya, Y. Stereoisomeric Bio-Inversion Key to Biosynthesis of Firefly d-Luciferin. *FEBS Lett.* **2006**, *580* (22), 5283–5287. https://doi.org/10.1016/j.febslet.2006.08.073.

(40) Nakamura, M.; Niwa, K.; Maki, S.; Hirano, T.; Ohmiya, Y.; Niwa, H. Construction of a New Firefly Bioluminescence System Using L-Luciferin as Substrate. *Tetrahedron Lett.* **2006**, *47* (7), 1197–1200. https://doi.org/10.1016/j.tetlet.2005.12.033.

(41) Niwa, K.; Nakajima, Y.; Ohmiya, Y. Applications of Luciferin Biosynthesis: Bioluminescence Assays for l-Cysteine and Luciferase. *Anal. Biochem.* **2010**, *396* (2), 316–318. https://doi.org/10.1016/j.ab.2009.09.014.

(42) Zhang, C.; Yuan, M.; Han, G.; Gao, Y.; Tang, C.; Li, X.; Du, L.; Li, M. Novel Caged Luciferin Derivatives Can Prolong Bioluminescence Imaging in Vitro and in Vivo. *RSC Adv.* **2018**, *8* (35), 19596–19599. https://doi.org/10.1039/C8RA02312C.

(43) Sondag, D.; Heming, J. J. A.; Löwik, D. W. P. M.; Krivosheeva, E.; Lejeune, D.; van Geffen, M.; van't Veer, C.; van Heerde, W. L.; Beens, M. C. J.; Kuijpers, B. H. M.; Boltje, T. J.; Rutjes, F. P. J. T. Solid-Phase Synthesis of Caged Luminescent Peptides via Side Chain Anchoring. *Bioconjug. Chem.* **2023**, *34* (12), 2234–2242. https://doi.org/10.1021/acs.bioconjchem.3c00381.

(44) Navarro, M. X.; Brennan, C. K.; Love, A. C.; Prescher, J. A. Caged Luciferins Enable Rapid Multicomponent Bioluminescence Imaging. *Photochem. Photobiol.* **2024**, *100* (1), 67–74. https://doi.org/10.1111/php.13814.

(45) Syed, A. J.; Anderson, J. C. Applications of Bioluminescence in Biotechnology and Beyond. *Chem. Soc. Rev.* **2021**, *50* (9), 5668–5705. https://doi.org/10.1039/D0CS01492C.

(46) Loy, C. A.; Trader, D. J. Caged Aminoluciferin Probe for Bioluminescent Immunoproteasome Activity Analysis. *RSC Chem. Biol.* **2024**, *5* (9), 877–883. https://doi.org/10.1039/D4CB00148F.

(47) Reddy, G. R.; Thompson, W. C.; Miller, S. C. Robust Light Emission from Cyclic Alkylaminoluciferin Substrates for Firefly Luciferase. *J. Am. Chem. Soc.* **2010**, *132* (39), 13586–13587. https://doi.org/10.1021/ja104525m.

(48) Godinat, A.; Budin, G.; Morales, A. R.; Park, H. M.; Sanman, L. E.; Bogyo, M.; Yu, A.; Stahl, A.; Dubikovskaya, E. A. A Biocompatible “Split Luciferin” Reaction and Its Application for Non-Invasive Bioluminescent Imaging of Protease Activity in Living Animals. *Curr. Protoc. Chem. Biol.* **2014**, *6* (3), 169–189. https://doi.org/10.1002/9780470559277.ch140047.

(49) Papadopoulos, A. O.; Ealand, C.; Gordhan, B. G.; VanNieuwenhze, M.; Kana, B. D. Characterisation of a Putative M23-Domain Containing Protein in Mycobacterium Tuberculosis. *PLOS ONE* **2021**, *16* (11), e0259181. https://doi.org/10.1371/journal.pone.0259181.

(50) Rodrigues, L.; Ramos, J.; Couto, I.; Amaral, L.; Viveiros, M. Ethidium Bromide Transport across Mycobacterium Smegmatis Cell-Wall: Correlation with Antibiotic Resistance. *BMC Microbiol.* **2011**, *11*, 35. https://doi.org/10.1186/1471-2180-11-35.

(51) Bisson, G. P.; Mehaffy, C.; Broeckling, C.; Prenni, J.; Rifat, D.; Lun, D. S.; Burgos, M.; Weissman, D.; Karakousis, P. C.; Dobos, K. Upregulation of the Phthiocerol

Dimycocerosate Biosynthetic Pathway by Rifampin-Resistant, rpoB Mutant Mycobacterium Tuberculosis. *J. Bacteriol.* **2012**, *194* (23), 6441–6452. https://doi.org/10.1128/JB.01013-12.

(52) Chuang, Y.-M.; Bandyopadhyay, N.; Rifat, D.; Rubin, H.; Bader, J. S.; Karakousis, P. C. Deficiency of the Novel Exopolyphosphatase Rv1026/PPX2 Leads to Metabolic Downshift and Altered Cell Wall Permeability in Mycobacterium Tuberculosis. *mBio* **2015**, *6* (2), 10.1128/mbio.02428-14. https://doi.org/10.1128/mbio.02428-14.

(53) Campodónico, V. L.; Rifat, D.; Chuang, Y.-M.; Ioerger, T. R.; Karakousis, P. C. Altered Mycobacterium Tuberculosis Cell Wall Metabolism and Physiology Associated With RpoB Mutation H526D. *Front. Microbiol.* **2018**, *9*. https://doi.org/10.3389/fmicb.2018.00494.

(54) Larsen, E. M.; Johnson, R. J. Microbial Esterases and Ester Prodrugs: An Unlikely Marriage for Combating Antibiotic Resistance. https://doi.org/10.1002/ddr.21468.

(55) Rautio, J.; Kumpulainen, H.; Heimbach, T.; Oliyai, R.; Oh, D.; Järvinen, T.; Savolainen, J. Prodrugs: Design and Clinical Applications. *Nat. Rev. Drug Discov.* **2008**, *7* (3), 255–270. https://doi.org/10.1038/nrd2468.

(56) Valente, E.; Testa, B.; Constantino, L. Activation of Benzoate Model Prodrugs by Mycobacteria. Comparison with Mammalian Plasma and Liver Hydrolysis. *Eur. J. Pharm. Sci.* **2021**, *162*, 105831. https://doi.org/10.1016/j.ejps.2021.105831.

(57) Larsen, E. M.; Stephens, D. C.; Clarke, N. H.; Johnson, R. J. Ester-Prodrugs of Ethambutol Control Its Antibacterial Activity and Provide Rapid Screening for Mycobacterial Hydrolase Activity. *Bioorg. Med. Chem. Lett.* **2017**, *27* (19), 4544–4547. https://doi.org/10.1016/j.bmcl.2017.08.057.

(58) Tallman, K. R.; Levine, S. R.; Beatty, K. E. Profiling Esterases in Mycobacterium Tuberculosis Using Far-Red Fluorogenic Substrates. *ACS Chem. Biol.* **2016**, *11* (7), 1810–1815. https://doi.org/10.1021/acschembio.6b00233.

(59) Tallman, K. R.; Levine, S. R.; Beatty, K. E. Small-Molecule Probes Reveal Esterases with Persistent Activity in Dormant and Reactivating Mycobacterium Tuberculosis. *ACS Infect. Dis.* **2016**, *2* (12), 936–944. https://doi.org/10.1021/acsinfecdis.6b00135.

(60) Pieters, J. *Mycobacterium Tuberculosis* and the Macrophage: Maintaining a Balance. *Cell Host Microbe* **2008**, *3* (6), 399–407. https://doi.org/10.1016/j.chom.2008.05.006.

(61) Ohkuma, S.; Poole, B. Fluorescence Probe Measurement of the Intralysosomal pH in Living Cells and the Perturbation of pH by Various Agents. *Proc. Natl. Acad. Sci.* **1978**, *75* (7), 3327–3331. https://doi.org/10.1073/pnas.75.7.3327.

(62) Vandal, O. H.; Nathan, C. F.; Ehrt, S. Acid Resistance in Mycobacterium Tuberculosis. *J. Bacteriol.* **2009**, *191* (15), 4714–4721. https://doi.org/10.1128/jb.00305-09.

(63) Sibley, L. D.; Franzblau, S. G.; Krahenbuhl, J. L. Intracellular Fate of Mycobacterium Leprae in Normal and Activated Mouse Macrophages. *Infect. Immun.* **1987**, *55* (3), 680–685. https://doi.org/10.1128/iai.55.3.680-685.1987.

(64) Via, L. E.; Fratti, R. A.; McFalone, M.; Pagán-Ramos, E.; Deretic, D.; Deretic1, V. Effects of Cytokines on Mycobacterial Phagosome Maturation. *J. Cell Sci.* **1998**, *111* (7), 897–905. https://doi.org/10.1242/jcs.111.7.897.

(65) Vandal, O. H.; Nathan, C. F.; Ehrt, S. Acid Resistance in Mycobacterium Tuberculosis. *J. Bacteriol.* **2009**. https://doi.org/10.1128/jb.00305-09.

(66) Vandal, O. H.; Roberts, J. A.; Odaira, T.; Schnappinger, D.; Nathan, C. F.; Ehrt, S. Acid-Susceptible Mutants of Mycobacterium Tuberculosis Share Hypersusceptibility to Cell Wall and Oxidative Stress and to the Host Environment. *J. Bacteriol.* **2009**. https://doi.org/10.1128/jb.00932-08.

(67) Laudouze, J.; Canaan, S.; Gouzy, A.; Santucci, P. Unraveling Mycobacterium Tuberculosis Acid Resistance and pH Homeostasis Mechanisms. *FEBS Lett.* **2025**, *599* (12), 1634–1648. https://doi.org/10.1002/1873-3468.70023.

(68) Rao, M.; Streur, T. L.; Aldwell, F. E.; Cook, G. M. Intracellular pH Regulation by Mycobacterium Smegmatis and Mycobacterium Bovis BCG. *Microbiology* **2001**, *147* (4), 1017–1024. https://doi.org/10.1099/00221287-147-4-1017.

(69) Early, J.; Ollinger, J.; Darby, C.; Alling, T.; Mullen, S.; Casey, A.; Gold, B.; Ochoada, J.; Wiernicki, T.; Masquelin, T.; Nathan, C.; Hipskind, P. A.; Parish, T. Identification of Compounds with pH-Dependent Bactericidal Activity against Mycobacterium Tuberculosis. *ACS Infect. Dis.* **2019**, *5* (2), 272–280. https://doi.org/10.1021/acsinfecdis.8b00256.

(70) Ando, Y.; Niwa, K.; Yamada, N.; Enomoto, T.; Irie, T.; Kubota, H.; Ohmiya, Y.; Akiyama, H. Firefly Bioluminescence Quantum Yield and Colour Change by pH-Sensitive Green Emission. *Nat. Photonics* **2008**, *2* (1), 44–47. https://doi.org/10.1038/nphoton.2007.251.

(71) Vandal, O. H.; Pierini, L. M.; Schnappinger, D.; Nathan, C. F.; Ehrt, S. A Membrane Protein Preserves Intrabacterial pH in Intraphagosomal Mycobacterium Tuberculosis. *Nat. Med.* **2008**, *14* (8), 849–854. https://doi.org/10.1038/nm.1795.

(72) Raynaud, C.; Papavinasasundaram, K. G.; Speight, R. A.; Springer, B.; Sander, P.; Böttger, E. C.; Colston, M. J.; Draper, P. The Functions of OmpATb, a Pore-forming Protein of Mycobacterium Tuberculosis.

(73) Hillmann, D.; Eschenbacher, I.; Thiel, A.; Niederweis, M. Expression of the Major Porin Gene mspA Is Regulated in Mycobacterium Smegmatis. *J. Bacteriol.* **2007**, *189* (3), 958–967. https://doi.org/10.1128/jb.01474-06.

(74) Rodrigues, L.; Ramos, J.; Couto, I.; Amaral, L.; Viveiros, M. Ethidium Bromide Transport across Mycobacterium Smegmatiscell-Wall: Correlation with Antibiotic Resistance. *BMC Microbiol.* **2011**, *11* (1), 35. https://doi.org/10.1186/1471-2180-11-35.

(75) Niederweis, M. Mycobacterial Porins – New Channel Proteins in Unique Outer Membranes. *Mol. Microbiol.* **2003**, *49* (5), 1167–1177. https://doi.org/10.1046/j.1365-2958.2003.03662.x.

(76) Stahl, C.; Kubetzko, S.; Kaps, I.; Seeber, S.; Engelhardt, H.; Niederweis, M. MspA Provides the Main Hydrophilic Pathway through the Cell Wall of Mycobacterium Smegmatis. *Mol. Microbiol.* **2001**, *40* (2), 451–464. https://doi.org/10.1046/j.1365-2958.2001.02394.x.

(77) Niederweis, M.; Ehrt, S.; Heinz, C.; Klöcker, U.; Karosi, S.; Swiderek, K. M.; Riley, L. W.; Benz, R. Cloning of the mspA Gene Encoding a Porin from Mycobacterium

Smegmatis. *Mol. Microbiol.* **1999**, *33* (5), 933–945. https://doi.org/10.1046/j.1365-2958.1999.01472.x.

(78) Dela Vega, A. L.; Delcour, A. H. Polyamines Decrease Escherichia Coli Outer Membrane Permeability. *J. Bacteriol.* **1996**, *178* (13), 3715–3721. https://doi.org/10.1128/jb.178.13.3715-3721.1996.

(79) Samartzidou, H.; Delcour, A. H. Excretion of Endogenous Cadaverine Leads to a Decrease in Porin-Mediated Outer Membrane Permeability. *J. Bacteriol.* **1999**, *181* (3), 791–798. https://doi.org/10.1128/jb.181.3.791-798.1999.

(80) CHEVALIER, J.; MALLÉA, M.; PAGÈS, J.-M. Comparative Aspects of the Diffusion of Norfloxacin, Cefepime and Spermine through the F Porin Channel of Enterobacter Cloacae. *Biochem. J.* **2000**, *348* (1), 223–227. https://doi.org/10.1042/bj3480223.

(81) Dai, T.; Xie, J.; Zhu, Q.; Kamariza, M.; Jiang, K.; Bertozzi, C. R.; Rao, J. A Fluorogenic Trehalose Probe for Tracking Phagocytosed Mycobacterium Tuberculosis. *J. Am. Chem. Soc.* **2020**, *142* (36), 15259–15264. https://doi.org/10.1021/jacs.0c07700.

(82) Sarathy, J. P.; Lee, E.; Dartois, V. Polyamines Inhibit Porin-Mediated Fluoroquinolone Uptake in Mycobacteria. *PLOS ONE* **2013**, *8* (6), e65806. https://doi.org/10.1371/journal.pone.0065806.

(83) Iyer, R.; Delcour, A. H. Complex Inhibition of OmpF and OmpC Bacterial Porins by Polyamines*. *J. Biol. Chem.* **1997**, *272* (30), 18595–18601. https://doi.org/10.1074/jbc.272.30.18595.

(84) Kumar, V.; Mishra, R. K.; Ghose, D.; Kalita, A.; Dhiman, P.; Prakash, A.; Thakur, N.; Mitra, G.; Chaudhari, V. D.; Arora, A.; Dutta, D. Free Spermidine Evokes

Superoxide Radicals That Manifest Toxicity. *eLife* **2022**, *11*, e77704. https://doi.org/10.7554/eLife.77704.

(85) Nguyen, P. P.; Kado, T.; Prithviraj, M.; Siegrist, M. S.; Morita, Y. S. Inositol Acylation of Phosphatidylinositol Mannosides: A Rapid Mass Response to Membrane Fluidization in Mycobacteria. *J. Lipid Res.* **2022**, *63* (9), 100262. https://doi.org/10.1016/j.jlr.2022.100262.

(86) Kado, T.; Akbary, Z.; Motooka, D.; Sparks, I. L.; Melzer, E. S.; Nakamura, S.; Rojas, E. R.; Morita, Y. S.; Siegrist, M. S. A Cell Wall Synthase Accelerates Plasma Membrane Partitioning in Mycobacteria. *eLife* **2023**, *12*, e81924. https://doi.org/10.7554/eLife.81924.

(87) Webber, M. A.; Piddock, L. J. V. The Importance of Efflux Pumps in Bacterial Antibiotic Resistance. *J. Antimicrob. Chemother.* **2003**, *51* (1), 9–11. https://doi.org/10.1093/jac/dkg050.

(88) Du, D.; Wang-Kan, X.; Neuberger, A.; van Veen, H. W.; Pos, K. M.; Piddock, L. J. V.; Luisi, B. F. Multidrug Efflux Pumps: Structure, Function and Regulation. *Nat. Rev. Microbiol.* **2018**, *16* (9), 523–539. https://doi.org/10.1038/s41579-018-0048-6.

(89) Stavri, M.; Piddock, L. J. V.; Gibbons, S. Bacterial Efflux Pump Inhibitors from Natural Sources. *J. Antimicrob. Chemother.* **2007**, *59* (6), 1247–1260. https://doi.org/10.1093/jac/dkl460.

(90) Duffey, M.; Jumde, R. P.; da Costa, R. M. A.; Ropponen, H.-K.; Blasco, B.; Piddock, L. J. V. Extending the Potency and Lifespan of Antibiotics: Inhibitors of Gram-Negative Bacterial Efflux Pumps. *ACS Infect. Dis.* **2024**, *10* (5), 1458–1482. https://doi.org/10.1021/acsinfecdis.4c00091.

(91) Johnson, E. O.; LaVerriere, E.; Office, E.; Stanley, M.; Meyer, E.; Kawate, T.; Gomez, J. E.; Audette, R. E.; Bandyopadhyay, N.; Betancourt, N.; Delano, K.; Da Silva, I.; Davis, J.; Gallo, C.; Gardner, M.; Golas, A. J.; Guinn, K. M.; Kennedy, S.; Korn, R.; McConnell, J. A.; Moss, C. E.; Murphy, K. C.; Nietupski, R. M.; Papavinasasundaram, K. G.; Pinkham, J. T.; Pino, P. A.; Proulx, M. K.; Ruecker, N.; Song, N.; Thompson, M.; Trujillo, C.; Wakabayashi, S.; Wallach, J. B.; Watson, C.; Ioerger, T. R.; Lander, E. S.; Hubbard, B. K.; Serrano-Wu, M. H.; Ehrt, S.; Fitzgerald, M.; Rubin, E. J.; Sassetti, C. M.; Schnappinger, D.; Hung, D. T. Large-Scale Chemical–Genetics Yields New M. Tuberculosis Inhibitor Classes. *Nature* **2019**, *571* (7763), 72–78. https://doi.org/10.1038/s41586-019-1315-z.

(92) Pasca, M. R.; Guglierame, P.; Arcesi, F.; Bellinzoni, M.; De Rossi, E.; Riccardi, G. Rv2686c-Rv2687c-Rv2688c, an ABC Fluoroquinolone Efflux Pump in Mycobacterium Tuberculosis. *Antimicrob. Agents Chemother.* **2004**, *48* (8), 3175–3178. https://doi.org/10.1128/aac.48.8.3175-3178.2004.

(93) Pasca, M. R.; Guglierame, P.; De Rossi, E.; Zara, F.; Riccardi, G. mmpL7 Gene of Mycobacterium Tuberculosis Is Responsible for Isoniazid Efflux in Mycobacterium Smegmatis. *Antimicrob. Agents Chemother.* **2005**, *49* (11), 4775–4777. https://doi.org/10.1128/aac.49.11.4775-4777.2005.

(94) Silva, P. E. A.; Bigi, F.; de la Paz Santangelo, M.; Romano, M. I.; Martín, C.; Cataldi, A.; Aínsa, J. A. Characterization of P55, a Multidrug Efflux Pump inMycobacterium Bovis and Mycobacterium Tuberculosis. *Antimicrob. Agents Chemother.* **2001**, *45* (3), 800–804. https://doi.org/10.1128/aac.45.3.800-804.2001.

(95) Danilchanka, O.; Pavlenok, M.; Niederweis, M. Role of Porins for Uptake of Antibiotics by Mycobacterium Smegmatis. *Antimicrob. Agents Chemother.* **2008**, *52* (9), 3127–3134. https://doi.org/10.1128/aac.00239-08.

(96) Copolovici, D. M.; Langel, K.; Eriste, E.; Langel, Ü. Cell-Penetrating Peptides: Design, Synthesis, and Applications. *ACS Nano* **2014**, *8* (3), 1972–1994. https://doi.org/10.1021/nn4057269.

(97) Madani, F.; Lindberg, S.; Langel, Ü.; Futaki, S.; Gräslund, A. Mechanisms of Cellular Uptake of Cell-Penetrating Peptides. *J. Biophys.* **2011**, *2011* (1), 414729. https://doi.org/10.1155/2011/414729.

(98) Peraro, L.; Deprey, K. L.; Moser, M. K.; Zou, Z.; Ball, H. L.; Levine, B.; Kritzer, J. A. Cell Penetration Profiling Using the Chloroalkane Penetration Assay. *J. Am. Chem. Soc.* **2018**, *140* (36), 11360–11369. https://doi.org/10.1021/jacs.8b06144.

(99) Stanzl, E. G.; Trantow, B. M.; Vargas, J. R.; Wender, P. A. Fifteen Years of Cell-Penetrating, Guanidinium-Rich Molecular Transporters: Basic Science, Research Tools, and Clinical Applications. *Acc. Chem. Res.* **2013**, *46* (12), 2944–2954. https://doi.org/10.1021/ar4000554.

(100) Fuchs, S. M.; Raines, R. T. Polyarginine as a Multifunctional Fusion Tag. *Protein Sci.* **2005**, *14* (6), 1538–1544. https://doi.org/10.1110/ps.051393805.

(101) Fuchs, S. M.; Raines, R. T. Pathway for Polyarginine Entry into Mammalian Cells. *Biochemistry* **2004**, *43* (9), 2438–2444. https://doi.org/10.1021/bi035933x.

(102) Nakase, I.; Konishi, Y.; Ueda, M.; Saji, H.; Futaki, S. Accumulation of Arginine-Rich Cell-Penetrating Peptides in Tumors and the Potential for Anticancer Drug Delivery *in*

Vivo. *J. Controlled Release* **2012**, *159* (2), 181–188. https://doi.org/10.1016/j.jconrel.2012.01.016.

(103) Antonoplis, A.; Zang, X.; Huttner, M. A.; Chong, K. K. L.; Lee, Y. B.; Co, J. Y.; Amieva, M. R.; Kline, K. A.; Wender, P. A.; Cegelski, L. A Dual-Function Antibiotic-Transporter Conjugate Exhibits Superior Activity in Sterilizing MRSA Biofilms and Killing Persister Cells. *J. Am. Chem. Soc.* **2018**, *140* (47), 16140–16151. https://doi.org/10.1021/jacs.8b08711.

(104) Li, Z.; Yang, Y.-J.; Qin, Z.; Li, S.-H.; Bai, L.-X.; Li, J.-Y.; Liu, X.-W. Florfenicol-Polyarginine Conjugates Exhibit Promising Antibacterial Activity Against Resistant Strains. *Front. Chem.* **2022**, *10*. https://doi.org/10.3389/fchem.2022.921091.

(105) Tang, M.; Waring, A. J.; Lehrer, R. I.; Hong, M. Effects of Guanidinium–Phosphate Hydrogen Bonding on the Membrane-Bound Structure and Activity of an Arginine-Rich Membrane Peptide from Solid-State NMR Spectroscopy. *Angew. Chem. Int. Ed.* **2008**, *47* (17), 3202–3205. https://doi.org/10.1002/anie.200705993.

(106) Robison, A. D.; Sun, S.; Poyton, M. F.; Johnson, G. A.; Pellois, J.-P.; Jungwirth, P.; Vazdar, M.; Cremer, P. S. Polyarginine Interacts More Strongly and Cooperatively than Polylysine with Phospholipid Bilayers. *J. Phys. Chem. B* **2016**, *120* (35), 9287–9296. https://doi.org/10.1021/acs.jpcb.6b05604.

(107) Brčić, J.; Tong, A.; Wender, P. A.; Cegelski, L. Conjugation of Vancomycin with a Single Arginine Improves Efficacy against Mycobacteria by More Effective Peptidoglycan Targeting. *J. Med. Chem.* **2023**, *66* (15), 10226–10237. https://doi.org/10.1021/acs.jmedchem.3c00565.

(108) Silva, T.; Magalhães, B.; Maia, S.; Gomes, P.; Nazmi, K.; Bolscher, J. G. M.; Rodrigues, P. N.; Bastos, M.; Gomes, M. S. Killing of Mycobacterium Avium by Lactoferricin Peptides: Improved Activity of Arginine- and d-Amino-Acid-Containing Molecules. *Antimicrob. Agents Chemother.* **2014**, *58* (6), 3461–3467. https://doi.org/10.1128/aac.02728-13.

(109) Bhandari, S.; Ongwae, G. M.; Dash, R.; Liu, Z.; Chordia, M. D.; He, Y.; Pires, M. M. Profiling Cytosolic Drug Delivery in Mammalian Cells: A Generalizable Assay for Intracellular Accumulation. bioRxiv June 6, 2025, p 2025.06.03.656700. https://doi.org/10.1101/2025.06.03.656700.

(110) Mitchell, D. j.; Steinman, L.; Kim, D. t.; Fathman, C. g.; Rothbard, J. b. Polyarginine Enters Cells More Efficiently than Other Polycationic Homopolymers. *J. Pept. Res.* **2000**, *56* (5), 318–325. https://doi.org/10.1034/j.1399-3011.2000.00723.x.

(111) Verdurmen, W. P. R.; Bovee-Geurts, P. H.; Wadhwani, P.; Ulrich, A. S.; Hällbrink, M.; van Kuppevelt, T. H.; Brock, R. Preferential Uptake of L- versus D-Amino Acid Cell-Penetrating Peptides in a Cell Type-Dependent Manner. *Chem. Biol.* **2011**, *18* (8), 1000–1010. https://doi.org/10.1016/j.chembiol.2011.06.006.

(112) Ma, Y.; Gong, C.; Ma, Y.; Fan, F.; Luo, M.; Yang, F.; Zhang, Y.-H. Direct Cytosolic Delivery of Cargoes *in Vivo* by a Chimera Consisting of D- and L-Arginine Residues. *J. Controlled Release* **2012**, *162* (2), 286–294. https://doi.org/10.1016/j.jconrel.2012.07.022.

(113) Hu, J.; Cochrane, W. G.; Jones, A. X.; Blackmond, D. G.; Paegel, B. M. Chiral Lipid Bilayers Are Enantioselectively Permeable. *Nat. Chem.* **2021**, *13* (8), 786–791. https://doi.org/10.1038/s41557-021-00708-z.

(114) Najjar, K.; Erazo-Oliveras, A.; Brock, D. J.; Wang, T.-Y.; Pellois, J.-P. An L- to d-Amino Acid Conversion in an Endosomolytic Analog of the Cell-Penetrating Peptide TAT Influences Proteolytic Stability, Endocytic Uptake, and Endosomal Escape*. *J. Biol. Chem.* **2017**, *292* (3), 847–861. https://doi.org/10.1074/jbc.M116.759837.

(115) Khara, J. S.; Priestman, M.; Uhía, I.; Hamilton, M. S.; Krishnan, N.; Wang, Y.; Yang, Y. Y.; Langford, P. R.; Newton, S. M.; Robertson, B. D.; Ee, P. L. R. Unnatural Amino Acid Analogues of Membrane-Active Helical Peptides with Anti-Mycobacterial Activity and Improved Stability. *J. Antimicrob. Chemother.* **2016**, *71* (8), 2181–2191. https://doi.org/10.1093/jac/dkw107.

(116) Lu, J.; Xu, H.; Xia, J.; Ma, J.; Xu, J.; Li, Y.; Feng, J. D- and Unnatural Amino Acid Substituted Antimicrobial Peptides With Improved Proteolytic Resistance and Their Proteolytic Degradation Characteristics. *Front. Microbiol.* **2020**, *11*. https://doi.org/10.3389/fmicb.2020.563030.

(117) Nakase, I.; Niwa, M.; Takeuchi, T.; Sonomura, K.; Kawabata, N.; Koike, Y.; Takehashi, M.; Tanaka, S.; Ueda, K.; Simpson, J. C.; Jones, A. T.; Sugiura, Y.; Futaki, S. Cellular Uptake of Arginine-Rich Peptides: Roles for Macropinocytosis and Actin Rearrangement. *Mol. Ther.* **2004**, *10* (6), 1011–1022. https://doi.org/10.1016/j.ymthe.2004.08.010.

(118) Pidgeon, S. E.; Apostolos, A. J.; Nelson, J. M.; Shaku, M.; Rimal, B.; Islam, M. N.; Crick, D. C.; Kim, S. J.; Pavelka, M. S.; Kana, B. D.; Pires, M. M. L,D-Transpeptidase Specific Probe Reveals Spatial Activity of Peptidoglycan Cross-Linking. *ACS Chem. Biol.* **2019**, *14* (10), 2185–2196. https://doi.org/10.1021/acschembio.9b00427.

(119) Patiño, S.; Alamo, L.; Cimino, M.; Casart, Y.; Bartoli, F.; García, M. J.; Salazar, L. Autofluorescence of Mycobacteria as a Tool for Detection of Mycobacterium Tuberculosis. *J. Clin. Microbiol.* **2008**, *46* (10), 3296–3302. https://doi.org/10.1128/JCM.02183-07.